UNIVERSITAT POLITÈCNICA DE VALÈNCIA

UNIVERSITAT POLITÈCNICA DE VALÈNCIA

Escuela Técnica Superior de Ingeniería Industrial

Liquid Hydrogen Pipeline Distribution at Airports. A Model-Based Assessment.

Trabajo Fin de Máster

Máster Universitario en Ingeniería Industrial-Màster Universitari en Enginyeria Industrial

AUTOR: Fanlo Escudero, Miguel

Tutores: Quijano López, Alfredo; Hormung, Mirko: Ebner, Kathrin

CURSO ACADÉMICO: 2023/2024

Chair of Aircraft Design
Lehrstuhl für Luftfahrtsysteme

Liquid Hydrogen Pipeline Distribution at Airports. A Model-Based Assessment

Master Thesis

Submitted in partial fulfillment of the requirements for the master M.Sc. Mechanical Engineering at the Department of Mechanical Engineering of the Technical University of Munich.

Supervised by	Prof. Dr.-Ing. Mirko Hornung; Chair of Aircraft Design Dr. Kathrin Ebner; Bauhaus Luftfahrt e.V.
Submitted by	Miguel Fanlo Escudero Student ID: 03770443
Submitted on	23. August 2023
Sequential number	LS-SA 23/03

Abstract

In the face of growing energy demand and the need to reduce greenhouse gases, green hydrogen represents an attractive energy vector that can decarbonize highly energy-demanding sectors, such as aviation. In particular, liquid hydrogen, due to its higher energy density per unit volume compared to its gaseous state, is expected to progressively replace traditional fuels in aviation. To make hydrogen-based aviation a reality, the aviation sector must undergo a major transformation from fully developing the hydrogen supply chain to redesigning existing aircraft and airport infrastructures. Due to the characteristics of liquid hydrogen, whose boiling point is -253°C, highly insulated technology must be developed along the supply chain to prevent boil-off. Boil-off is the vaporization of the fuel due to unavoidable heat input and represents a challenge as it can significantly impact on the overall efficiency of the LH_2 supply chain.

This thesis provides preliminary knowledge on the distribution of liquid hydrogen by pipeline at the airport. The boundaries of the study include the distribution of hydrogen from the airport storage farm to each aircraft stand. The study focuses only on fuel transfer, excluding subsequent refueling. To do this a generic airport is defined taking into account expected performance parameters and characteristics of each of the main components of the pipeline distribution system. The work focuses on quantifying the volume of boil-off gases occurring along the distribution pipeline under base case operating conditions and employs this parameter for a comparative assessment. Next, a series of parametric analyses are performed in which the impact of several parameters on the boil-off are evaluated and the results are compared with the base case.

This thesis, although a preliminary study, can serve as a simplified model to compare different configurations and assist in infrastructure design decisions. In addition, the work highlights the need for further research and development of technologies and equipment to be able to implement hydrogen in aviation.

Keywords: liquid hydrogen, airport, pipeline distribution, boil-off gases.

.

Acknowledgement

First, I would like to thank my supervisors, Prof. Dr.-Ing. Mirko Hornung and Dr. Kathrin Ebner, for the opportunity to perform this work and for the trust placed in me. Especially to Dr. Kathrin Ebner, who passed on to me her enormous passion for the subject from the very first moment. Furthermore, her support and dedication have been fundamental throughout this thesis, and I feel that I have learned many valuable lessons from her. For me, it has been a pleasure to work with her and I wish her all the best for the future.

Secondly, I would also like to thank Dr. Alfredo Quijano, for having endorsed this work on behalf of the UPV and my friend Razvan Stoica for his interest and help in the thesis.

Then, I would like to thank my family for their unconditional support. Thank you for allowing me to study abroad and instilling curiosity in me. In particular, I dedicate this work to my mother. Despite the distance, I have felt her very close. Heartfelt thanks to Marián for her love and patience.

Finally, thank you to all the people I have met in Munich, from my colleagues at Studentenstadt, to my colleagues at Bauhaus Luftfahrt e.V., to the many friends that ERASMUS+ has given me. Moreover, thank you to the Universidad Politécnica de Valencia and the Technical University of Munich for making this exchange experience so enjoyable.

Table of contents

List of Figures

List of Tables

Glossary

Abbreviations

ATAG …… Air Transport Action Group
BO ……. Boil-Off
cGH_2 ……. Compressed Hydrogen
EU ……. European Union
GH_2 ……... Gaseous Hydrogen
GHG ……. Green Houses Gases
HLP ……..…… Hydrogen Liquefaction Plant
IEA …… International Energy Agency
LH_2 …… Liquid Hydrogen
LHV ……..…. Lower Heating Value
MLI ……..... Multilayer insulation
SAF …….. Sustainable Aviation Fuel
SMR ……. Steam Methane Reforming

1. Introduction

The current fossil fuel-based economy model is responsible for the emission of enormous amounts of CO_2 directly related to the combustion of fossil, carbon-based energy carriers. The ongoing increase in greenhouse gas emissions from human activity is leading to a worldwide worrying climate situation that threatens life on Earth. The following figure presents the evolution of global GHG emissions from fuel combustion per product during the last fifty years.

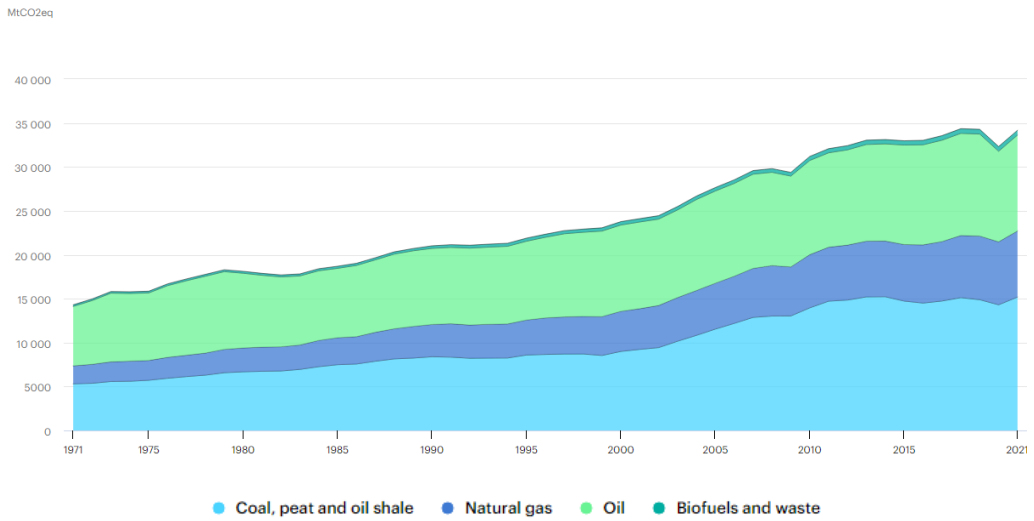

Figure 1.1*:* World GHG emissions from fuel combustion per product between 1971-2021 measured in equivalent megatons of CO_2. Adapted from IEA, (2023). [Open Access]

As the figure shows, CO_2 emissions have followed a ramp-up tendency since 1971, and the emission rate has increased considerably in the XXI century. This tendency is expected to continue due to the increasing world population and the acquisition of better life standards in developing countries.

Regarding sectors, transport is a very significant contributor to global warming. In particular, aviation is responsible for a considerable share of CO_2 emissions within the transport sector. In 2019, aviation CO_2 emissions represented about 2.5% of the global amount (McKinsey & Company, 2020). This share is even higher in the EU, where the aviation sector produced 5% of the total CO_2 emissions in 2019 (EU Aviation Safety Agency et al., 2022). An industry study has found that a 4% annual aviation demand growth is expected until 2050 (McKinsey & Company, 2020). This scenario suggests that, despite future efficiency improvements, emissions from aviation will double by 2050 compared to current values. To avoid this situation and in an effort to adhere to the Paris Agreement, limiting temperature rise to 1.5ºC by the end of the century compared to preindustrial values (United Nations, 2015), the European Commission presented its Green Deal (European Comission, 2019). This deal sets an ambitious decarbonization objective: achieving net carbon neutrality across all sectors and EU member states by 2050.

Figure 1.2 shows the forecast of CO2 emissions in aviation up to 2050 and distinguishes between different scenarios depending on the effectiveness of the measures adopted.

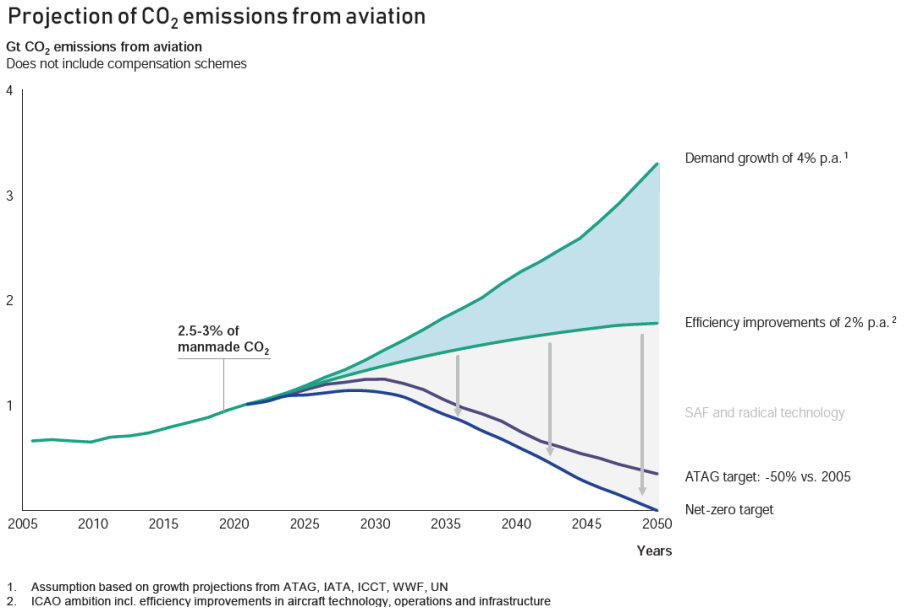

Figure 1.2: Projection of CO_2 emissions from aviation for the following decades (McKinsey & Company, 2020).

The first curve indicates that if aviation keeps growing at the current rate and no changes in practices and fuels are introduced, CO_2 emissions will exceed 3 Gt by 2050. The second curve represents how the first scenario's emissions can be reduced if technology and better practices improve efficiency at a 2% rate yearly. Nevertheless, aviation would still be far from reaching the decarbonization goals, both the ATAG target and the Green Deal one. Therefore, it is urgent to gradually stop relying on fossil fuels and invest great efforts in developing reliable alternatives.

Green hydrogen, sustainable aviation fuels (SAFs) and electricity-powered systems are expected to replace traditional kerosene as aviation fuel in the following decades. As an intrinsically carbon-free energy carrier liquid hydrogen, LH_2, holds great promise for decarbonization if produced from renewable, low emission-intensity electricity. Nonetheless, the challenges ahead to achieving hydrogen-based aviation are numerous and demanding, from producing low-carbon hydrogen at a competitive price, through hydrogen transport and distribution, to redesigning airport infrastructure and aircraft. Moreover, while an overall reduction of emission intensity as compared to kerosene combustion is expected, there are significant uncertainties when it comes to the climate impact of high-altitude emissions of the LH_2-aircraft. To lever the potential of green hydrogen for the aviation sector, there are currently numerous development and research activities ongoing.

1.1. Research gap

The need to drastically reduce greenhouse gas emissions in aviation makes green hydrogen, and especially liquid hydrogen, an attractive alternative to current fuels. However, further research is needed to make hydrogen-based aviation a reality, from redesigning aircraft and airport facilities to developing and deploying the entire hydrogen supply chain. With respect to liquid hydrogen, handling is complexed as it is a cryogenic fluid. In-depth analyses along the LH_2 supply chain are necessary. Special attention should be paid to the study of boil-off gases. As boil-off gases directly translate into overall efficiency along the LH_2 chain and, furthermore, the co-presence of gaseous species complexifies LH_2 storage, transport and transfer. In this line, it is not clear which

is the most efficient LH_2 distribution method at the airport as the technology and equipment required still have very low TRLs (Postma-Kurlanc et al., 2022) and only few theoretical assessments have been made.

1.2. Objectives

The thesis aims to provide preliminary knowledge on the distribution of LH_2 by pipeline at the airport, taking into account expected performance parameters and characteristics of each of the main components and the resulting boil-off gases along the distribution system. Thus, this work represents a simplified model-based assessment of the distribution of liquid hydrogen via pipeline at airports. One of the challenges presented by the use of a cryogenic fluid is the boil-off phenomenon, which is the vaporization of the fluid due to unwanted heat input. Thus, the work focuses on quantifying the volume of boil-off gases occurring along the pipeline distribution under generic operating conditions of an average airport employing this parameter for a comparative assessment. The boundaries of the study are set from the airport storage farm to the aircraft stand, where refueling takes place. Therefore, the analysis is limited to the performance of the main distribution pipeline, not considering the requirements or boil-off gases associated to aircraft refueling or LH_2 supply to the airport. The final objective of the thesis is helping to understand how significant boil-off gases can be in LH_2 pipeline distribution and which factors of the system must be considered to minimize the boil-offs when sizing a new airport infrastructure.

A generic airport scenario is defined based on data from bibliographic research. The modeled airport has no physical layout and, although it is located in the vicinity of Munich, it does not correspond to any real airport. To carry out the study, a simplified mathematical model is built and the performance of the distribution system is analyzed under different pipe diameters. After selecting the optimum size of the pipeline, a series of parametric analyses is carried out to evaluate the impact of certain parameters on the boil-off gases. Some of the analyzed parameters are the level of insulation, the ambient temperature, the pipe length and the mass flow delivered. The mathematical model and the calculations are implemented through a Matlab code.

2. State of the art

This chapter summarizes the state-of-the-art of research on hydrogen-based aviation. First, reasons why hydrogen, especially in its liquid state, is considered a promising energy carrier for decarbonizing aviation are presented. Continuedly, the hydrogen supply chain before the airport is addressed, from H_2 production to transport to the airport. Then, concepts for liquid hydrogen handling at the airport is described, from storage to distribution and aircraft refueling. Particular focus is put on distribution options, pointing out their advantages and disadvantages.

2.1. Potential of hydrogen in aviation

First, the characteristics that make hydrogen an attractive fuel option for aviation, both from an environmental point of view and in terms of its physical properties, are presented.

2.1.1. Climate impact of hydrogen-based aviation

Once analyzed the current climate scenario and decarbonization goals, there is no doubt that the climate impact of fuels used must be considered when designing future aviation. In this line, hydrogen is a potential solution. The central aspect is that the energy contained in hydrogen, H_2, can be obtained by combustion or through electrochemical reactions with no direct carbon emissions.

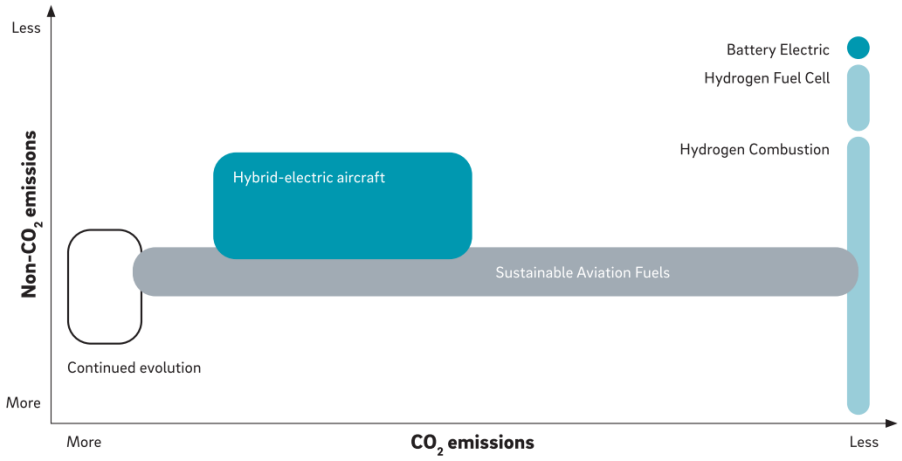

Figure 2.1: Expected environmental impact of different propulsion alternatives for aviation. Adapted from Thomson et al. (2020).

The figure above compares the emissions caused by the leading aircraft propulsion alternatives, including non-CO_2 and CO_2 emissions. It is crucial to remember that current aviation produces other emissions beyond CO_2. Nitrogen oxides (NO_x), soot, and water vapor, which create contrails and cirrus clouds, are emitted during kerosene combustion, too. Therefore, the total contribution of aviation emissions to global warming is considerably more significant than just considering CO_2 impact (McKinsey & Company, 2020).

Figure 2.1 shows that the most climate-friendly alternative in this line is electric-battery-propulsion aircraft because it reduces direct-flight emissions to zero. Despite this, batteries have a very low gravimetric energy density, which means heavy components would be needed to meet aircraft energy demands. Thus, they are expected to be limited

to short-range flights and are not considered a feasible alternative for decarbonizing the bulk of aviation traffic.

Then, SAFs exhibit great potential for reducing life-cycle CO_2 emissions if carbon capture processes are involved in their production, boosting carbon neutrality. On the contrary, non-CO_2 emissions remain close to current kerosene combustion levels with the exact volume depending on their chemical composition. The same applies to hybrid-electric aircraft, which in most studies focusing on commercial aviation it was found that emissions are only slightly reduced due to significantly increased weight from batteries and auxiliaries.

Last, hydrogen-based options bring direct-flight CO_2 emissions to zero and non-CO_2 emissions are reduced to water vapor only. The exact high-altitude climate impact of the latter is associated with significant uncertainties (Lee et al., 2021) and a matter of investigation. This reduction is believed to be more remarkable in fuel cell-powered aircraft than in direct combustion configurations due to the different characteristics of water emission (Adler & Martins, 2023). Unlike batteries, hydrogen has a high gravimetric energy density, so it can be a feasible solution for decarbonizing longer-range flights and a vast share of aviation.

2.1.2. Properties of hydrogen

Hydrogen is an energy carrier. It only exists in the Earth's atmosphere in insignificant quantities but can be produced through different methods. At atmospheric temperature and pressure, H_2 is found in gaseous form. Compared to kerosene, the specific energy density of H_2 is three times higher (Postma-Kurlanc et al., 2022). This aspect makes green hydrogen, produced from low-carbon techniques, a potential solution to decarbonize high energy-intensive sectors such as aviation, shipping, or metalworking.

However, due to its low density, H_2 must be compressed or liquified to reach reasonable volumetric energy densities. For this reason, liquid hydrogen (LH_2), which has a greater volumetric energy density than the gaseous state, is considered more appropriate for deployment in commercial aviation (Postma-Kurlanc et al., 2022). The downside is that LH_2 is a cryogenic liquid and must be kept below -252.7 ºC (20.4 K). Therefore, highly insulated systems are needed to store and transport LH_2 and prevent boil-off.

Table 2.1 shows how the density of hydrogen varies with temperature and pressure. These values help to understand why LH_2 is more likely to be used in commercial applications than gaseous hydrogen.

Table 2.1: Density of hydrogen at different temperatures and pressures (H2 Tools, 2023).

$\boldsymbol{Conditions\ of\ hydrogen}$	$\boldsymbol{Density\ (kg/m3)}$
Gaseous hydrogen, H_2 (1 bar, 0 ºC)	0.09
H_2 (300 bar, 0 ºC)	22.15
H_2 (1000 bar, 0 ºC)	52.12
Liquid hydrogen, LH_2 (1 bar, -253 ºC)	70.8

Table 2.2 sums up the properties of kerosene and LH_2. The table shows that even though hydrogen has a higher energy content per mass than kerosene, the volumetric energy density of LH_2 is only one-quarter of kerosene's. Therefore, to bring the same amount of energy onboard, larger storage facilities are needed for similar aircraft, which is a significant drawback as onboard space on a plane is limited. This aspect will require a considerable and challenging redesign of conventional airframes (IATA, 2019).

Table 2.2 Comparison of the properties of kerosene and liquid hydrogen (HFTO, 2023).

$\boldsymbol{Properties}$	$\boldsymbol{Kerosene}\ (\mathbf{1\ bar, 288\ K})$	$\boldsymbol{LH2}\ (\mathbf{1\ bar, 20\ K})$
Specific energy density (LHV)	42.8 MJ/kg	120 MJ/kg
Density	800 kg/m^3	71 kg/m^3
Volumetric energy density	34,240 MJ/m^3	8,520 MJ/m^3

Regarding fuel handling and safety, some aspects must be taken into account when working with hydrogen. First, H_2 is colorless, odorless, tasteless, and non-toxic. It is highly flammable due to its wide flammable range, high flame velocity and low ignition energy. This aspect is counterbalanced by its high buoyancy and low density, limiting pooling if a LH_2 spill occurs as it rapidly vaporizes and disperses. On the other hand, H_2 burns with an almost invisible bluish flame, which makes leak and fire detection difficult. Moreover, due to its high diffusivity, H_2 can easily leak through cracks or pores, causing material embrittlement and increasing the chance of failure. Therefore, high-performance insulation and embrittlement-resistant materials must be used in tanks, pipelines, and the rest of the H_2 facilities. Lastly, although liquid hydrogen itself does not burn, cryogenic boil-off leaks can cause severe cold burns in contact with people's skin (IATA, 2019; IEA, 2019; Postma-Kurlanc et al., 2022).

2.2. Production of hydrogen

Global hydrogen demand reached 94 Mt in 2021. Most of the current hydrogen production depends on fossil fuels, such as natural gas, coal, and oil. This means a yearly release of more than 900 Mt of CO_2 emissions (IEA, 2022), which implies a significant negative impact on climate. Oil refining, ammonia manufacture for fertilizers and rocket fuel are the main sectors demanding hydrogen (IEA, 2019).

A wide hydrogen color sort has been defined depending on which sources and techniques are used in hydrogen generation. Some of the main categories are presented. Today the most common process is steam methane reforming (SMR), which obtains hydrogen by splitting carbon from the methane molecule. This method uses natural gas as feedstock and produces the so-called gray hydrogen (Postma-Kurlanc et al., 2022). Then, if CO_2 emissions from SMR are captured and stored instead of released into the atmosphere, H_2 is categorized as blue hydrogen. This type reduces the carbon footprint but still relies on fossil fuels and extractive processes (IEA, 2019).

Last, green hydrogen is referred to hydrogen produced from renewable electricity. Electricity from sources such as wind or PV energy is used to power electrolysis. This process requires electricity to split hydrogen from the water molecule, releasing oxygen as a by-product. Unfortunately, today low-carbon hydrogen represents a tiny share, less

than 1% of the 2021 global production (IEA, 2022). Pink hydrogen from nuclear electricity can also be considered a low-carbon technology because no direct emissions are released during its production.

Only low-carbon hydrogen should be used in aviation to make decarbonization truly effective over the whole fuel life cycle. This is due to the fact that although the use of gray hydrogen in aviation would not produce direct CO_2 emissions during flight, CO_2 would be emitted upstream in the production process. To be more precise, CO_2 emissions ranging from 7.5 to 12 tons are typically generated to produce one ton of gray hydrogen via SMR (Katebah et al., 2022). Therefore, this is not a solution for decarbonizing aviation. In turn, green or pink hydrogen normally present a lower carbon footprint as emissions are mainly related to hydrogen transportation, compression or further conversion into hydrogen derivatives .

Another aspect that must be considered is production costs. Today, electrolysis costs are a considerable barrier, making low-carbon hydrogen way more expensive than grey hydrogen. Current fossil-fuel hydrogen prices range from 2 to 3 €/kg H_2. On the contrary, green hydrogen retail prices in road mobility are not expected to drop to around 5-7€/kg H_2 till 2030 (Jovan et al., 2020). This price would be higher in the case of liquid hydrogen as another energy intense production step is added with liquefaction. Therefore, there is still a long path ahead for hydrogen to be economically viable. Economies of scale and mass installation of renewable energies will gradually reduce electricity and equipment costs in the following decades, making hydrogen-based aviation feasible by the year 2050 (Hoelzen et al., 2022).

2.3. Hydrogen supply to the airport

From now on, low-carbon hydrogen will be referred to simply as hydrogen or H_2. Due to its very low density, hydrogen transportation and storage over long distances or periods mean a great challenge. Several transportation solutions are considered, such as gas pipelines or transport of cGH_2 or LH_2 vessels through trucks, trains and ships. Transportation of H_2 through various derivatives such as ammonia or hydrocarbons is also contemplated (IEA, 2019).

In the case of aviation, three likely scenarios for supplying H_2 to the airport are assumed, considering the airport's size, location, and demand (Adler et al., 2023; Postma-Kurlanc et al., 2022). The first scenario is the simplest one. In this case, hydrogen is generated and liquefied off-site, and then, LH_2 is supplied to the airport by road tankers. Supplying via rail tank cars or ships would be viable in certains scenarios. LH_2 is stored in the storage tank farm of the airport, which must have enough capacity to buffer a minimum three-day demand in case of supply disruption (Hoelzen et al., 2022). This scenario will likely occur in most airports during the first years of hydrogen introduction in aviation, not before 2035, as it presents the lowest capital investment (Postma-Kurlanc et al., 2022).

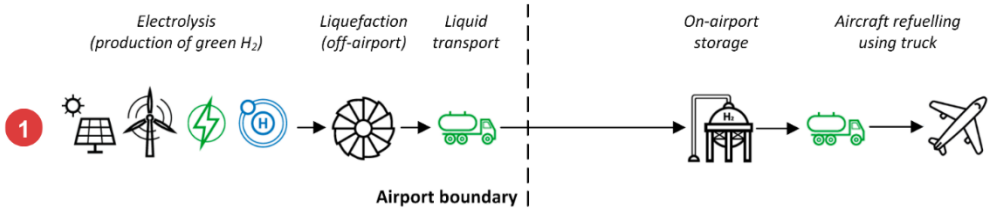

Figure 2.2: Scenario 1. Liquid hydrogen is produced off-site and transported by road tankers to the airport. Adapted from Adler et al. (2023).

If the hydrogen demand grows, many road tankers will be needed, which may cause traffic congestion and safety problems at the airport. Consequently, the second supply scenario deals with this problem. In this second case, hydrogen is produced off-site and transported to the airport through a gas pipeline. A hydrogen liquefaction plant, HLP, is placed on-site, transforming gas H_2 into liquid hydrogen. Then the fuel is sent to the storage tanks. This scenario will be suitable for medium to large airports in a more developed phase of hydrogen implementation, from 2040 onwards (Postma-Kurlanc et al., 2022). The viability of this scenario will also depend on local electricity cost.

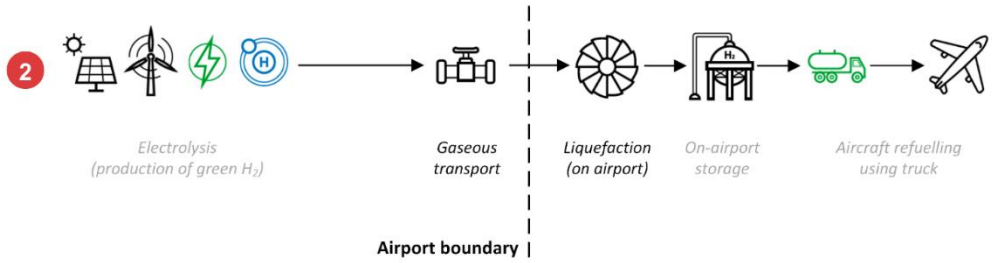

Figure 2.3: Scenario 2. Hydrogen is transported through a gas pipeline to the airport, where is liquefied. Adapted from Adler et al. (2023).

The last supply case consists of generating by electrolysis and liquefying hydrogen on-site, at the airport facilities. This scenario would require a large supply of electricity and vast space at the airport. Therefore, this scenario is only relevant in rare cases, where those conditions can be fulfilled.

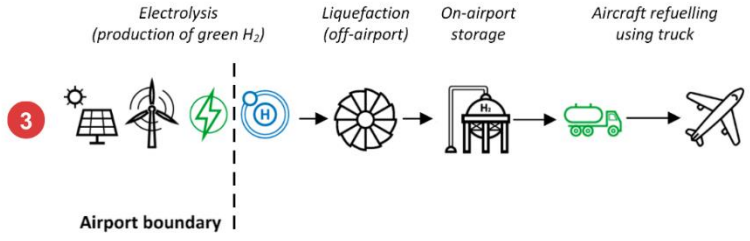

Figure 2.4: Scenario 3. The whole liquid hydrogen generation occurs at the airport from electrolysis to liquefaction and storage. Adapted from Adler et al. (2023).

Hence, the first two scenarios are likely more feasible for a larger share of airports. In the beginning, the implementation of hydrogen at all airports will be through road tankers,

and gradually, the second scenario will be deployed in medium and large airports. Road tankers supply will remain for small airports and as an emergency backup.

Brewer (1976) describes a different supply scenario for the airport of San Francisco. The report agrees that the second scenario is the most economical supply solution, i.e., locating the liquefaction plant at the airport. However, if building the liquefier at the airport site is impossible, due to space requirements or other aspects, Brewer (1976) states that the best alternative is to transport LH_2 from a nearby HLP up to 40 miles far, through a vacuum-jacketed pipeline. A first supply scenario should be adopted if the HLP is located further than 40 miles. Brewer compares supplying by rail tank cars and road tankers and claims that the former is more economical because a larger load is transported in each trip, reducing fillings and boil-off losses.

Regarding the hydrogen liquefaction process, some remarks must be made, as it represents a crucial step in the supply chain for hydrogen-based aviation to become a reality. Hydrogen liquefaction is an energy-intensive process in which the boiling point of hydrogen must be reached. That means cooling hydrogen to a cryogenic temperature of around 20 K (-253ºC). Concerning energy consumption, current processes require between 11.9 and 15 kWh/ kg LH_2, which would equal 35 to 45 % of the specific energy content of hydrogen (LHV: 33.3 kWh/kg) (Al Ghafri et al., 2022). Obviously, electricity used in the process should come from renewable sources to decarbonize the whole supply chain. Two different process designs are distinguished for large-scale industrial applications: the Claude process and Brayton refrigeration cycles. Even though the former has higher investment costs, it is the most established technique, providing better process efficiency and, thus, lower operating costs (Hoelzen et al., 2022). The current specific liquefaction cost ranges from 2.5 to 3 US$/kg LH_2, supposing a significant challenge for hydrogen-based aviation to be economically viable (Al Ghafri et al., 2022).

Another challenge of working with LH_2 as an energy carrier is dealing with cryogenic losses. During storage, transportation, and handling of LH_2, up to 40% of the total energy can be wasted through boil-off losses (Al Ghafri et al., 2022). Therefore, great efforts must be put into developing high-insulated equipment and facilities to reduce boil-off and optimize supply chain efficiency. The following chapter describes LH_2's state-of-the-art storage and handling techniques.

2.4. Handling of the liquid hydrogen at the airport

This section addresses LH_2 handling once the fuel has arrived at the airport. The liquid hydrogen handling has been divided into three consecutive processes: storage, distribution, and aircraft refueling. The objective is to deliver the cryogenic fuel from the storage farm to the aircraft tank. The main methods, techniques and components required for this task are described below.

2.4.1. LH_2 storage

Regardless of the supply method, LH_2 must be stored at the airport. Therefore, high-thermal-performance tanks are needed to minimize liquid hydrogen boiling, especially during long-term storage. The most commonly used tank designs are double-walled vacuum insulation vessels. Spherical-shaped tanks are recommended for large volumes as they provide the minimum surface-to-volume ratio, reducing heat transfer and resulting in a more uniform distribution of stresses and strains (Al Ghafri et al., 2022). Double-walled vacuum insulation consists of a cold inner tank in direct contact with the cryogenic liquid, a warm outer tank at ambient temperature, and an evacuated annulus in between containing the insulation material (Brewer, 1976). Internal structural supports,

such as rods, cables or load-bearing pods, are implemented to connect inner and outer tanks (Al Ghafri et al., 2022).

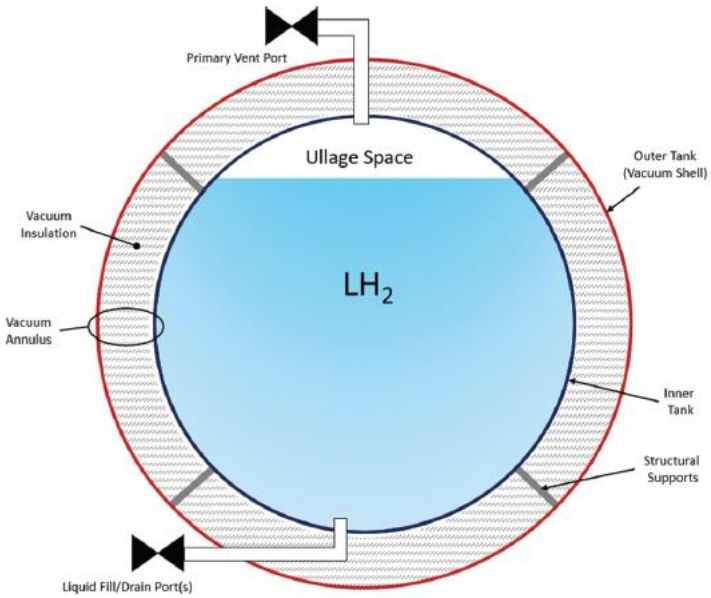

Figure 2.5: A schematic description of a LH_2 storage tank (Al Ghafri et al., 2022). [Open Access]

If one litre of LH_2 vaporizes at ambient pressure, it will occupy a volume of 845 litres (Postma-Kurlanc et al., 2022). Excessive boil-off gases will cause a significant pressure rise, and part of the gas must be vented off the storage tank. Therefore, as seen in Figure 2.5, storage tanks must always have an ullage space (below 10% of the total volume) and a relief valve to avoid overpressures (Al Ghafri et al., 2022).

Selecting the right materials is crucial to achieving the best performance of the storage tanks. A demanding trade-off is required between strength, fracture toughness, stiffness, cryogenic temperature resistance and low liquid and gaseous hydrogen permeation (Mital et al., 2006). As stationary ground-based storage facilities are not weight-constrained, tank walls can be composed of metal monolithic material. Austenitic stainless steel is typically used for the inner tank wall, whereas carbon steel is for the outer shell wall (Brewer, 1976). Inner walls can also be made of monels, aluminium and titanium alloys (Mital et al., 2006). Lighter solutions are being studied for aircraft tanks consisting of composite materials and liners (Xu et al., 2015).

Regarding insulation material, low thermal conductivity, low emissivity, low diffusivity and low coefficient of thermal expansion are some of the key properties required (Mital et al., 2006). In addition, a high vacuum level between the inner and outer vessels helps to minimize heat transfer. Depending on the insulation material, the vacuum level required can differ considerably. Traditionally, perlite powder has been used as insulation (Al Ghafri et al., 2022), but different solutions are being developed, such as aerogels, multilayer and microspheres insulations (Mital et al., 2006). A special focus is made on multilayer insulation, as is the option studied in this thesis.

Multilayer insulation, MLI, consists of alternating layers of low-emissivity metal foil (normally aluminised Mylar by DuPont) and a thin, low-conductance spacer (usually polyester or glass fiber paper) (Brewer, 1976). These layers work as thermal radiation

shields perpendicularly arranged to the heat flow direction (Mital et al., 2006). Mital et al. (2006) state that MLI systems provide a very low thermal conductivity, ranging from 10^{-5} to 10^{-8} W/mK. However, achieving this thermal performance requires maintaining a high vacuum, below 13 mPa.

Today, the largest LH_2 storage tank (3,200 m^3) was constructed in the mid-1960s by NASA and is located at the Kennedy Space Centre, FL, USA. At 22 K and 0.15 MPa storage conditions, it has a storage capacity of 263 tons of LH_2. This tank uses vacuum-perlite insulation and has a daily boil-off rate of 0.0625% of its total capacity. Recently, NASA announced that the construction of a larger storage tank is almost finished. The new LH_2 tank will have a total volume of 4732 m^3 and 327 tons of LH_2 capacity. It will be equipped with an evacuated glass bubbles insulation system that will reduce the boil-off rate to 0.03% per day. An Integrated Refrigeration and Storage (IRAS) heat exchanger will also be included to improve thermal control of the storage capability . These boil-off rates are similar to other values extracted from manufacturers and authors, such as Linde's largest tank (<0.1% per day) (Al Ghafri et al., 2022) or Brewer's study (Brewer, 1976). In all cases, boil-off losses are expected to be recovered and re-liquefied or used to feed hydrogen-based applications at the airport such as ground vehicles or heating.

As mentioned, the storage farm must have enough capacity to provide daily airport demand for at least three days in case of supply disruption (McKinsey & Company, 2020). Most authors agree that constructing aboveground tanks presents more advantages than underground tanks, as the former option is cheaper and easier to replace at the end of the tank's working life (Boeing, 1976; Brewer, 1976). Moreover, underground facilities increase the danger of generating trapped volumes of gaseous H_2 in the space provisioned for maintenance labors. This aspect increases the chance of detonation and reduces safety compared to aboveground tanks . On the contrary, the main benefits of locating tanks underground are removing them as an obstacle to flight traffic and reducing pipework (Postma-Kurlanc et al., 2022).

Lastly, depending on the LH_2 transfer method, the characteristics of the storage tanks will be different. If the flow is generated by pressure differential between the storage tank and the receiving vessel, the storage tank must be pressurizable. If, on the contrary, a cryogenic pump is used to feed LH_2, the storage tank can work at close to ambient pressure. Further discussion about both feeding alternatives is continued in the following chapter, which is focused on LH_2 distribution at the airport.

2.4.2. LH_2 distribution at the airport

The distribution of liquid hydrogen at the airport consists of delivering the fuel from the storage farm to the aircraft stand. As in the current kerosene distribution, two methods can be distinguished: by refueling trucks (or tankers) and by a pipeline and hydrant system.

2.4.2.1. LH_2 distribution by refueling trucks

Refueling trucks will be the most suitable distribution method at airports for small amounts during the introduction of hydrogen in aviation. It is a flexible option as the number of tankers can be easily adapted to the demand fluctuations, and it requires lower investment than a hydrant system. Hoelzen et al. (2022) claim that refueling trucks are the most economical solution for airports with demands lower than 125 kt LH_2 per year, i.e., roughly 342 tons of LH_2 per day. If demand exceeds this value, tankers may cause traffic congestion on the airport apron, with consequent safety concerns.

Moreover, as the LH_2 volume in a tanker is limited, a large fleet of vehicles would be required, demanding vast space needs at the airport. And last, due to the lower energy density of LH_2 by volume compared to kerosene, larger or multiple tankers would be required during the aircraft refueling. This could disturb other ground support vehicles' operation during turnaround processes, leading to an overall increase in turnaround times.

The capacity of the tankers will depend on the aircraft size, ranging from 20 m^3 for small aircraft (Postma-Kurlanc et al., 2022) up to 70 m^3 for the largest planes (Mangold et al., 2022). An additional 4% of the LH_2 usable tanker capacity must always remain in the tank to keep it cool (Hoelzen et al., 2022). Emptying the tankers completely would lead to large boil-off related to the required chill-down before refilling them again. In Boeing (1976), boil-off gases produced during distribution and aircraft refueling by tankers are vented to the atmosphere, leading to considerable economic waste and large GH_2 emissions. On the contrary, with coming technology, boil-off will be stored in tankers and even used to power them (Lopez, 2022; Mangold et al., 2022), increasing process efficiency. As shown in Figure 2.6, if the purging process is required tankers also need to carry helium on board. Helium is sometimes used to purge the refueling hose and the aircraft tank before the refueling starts. At cryogenic temperature, foreign substances can freeze in the hose blocking it. Therefore, pressurized helium, whose boiling point is 4.2 K, is used to eliminate any frozen particles in the refueling hose. A significant downside of helium purging is that helium is an expensive and non-renewable gas. Thus, helium recycling is essential to establish LH_2 as a fuel (Mangold et al., 2022).

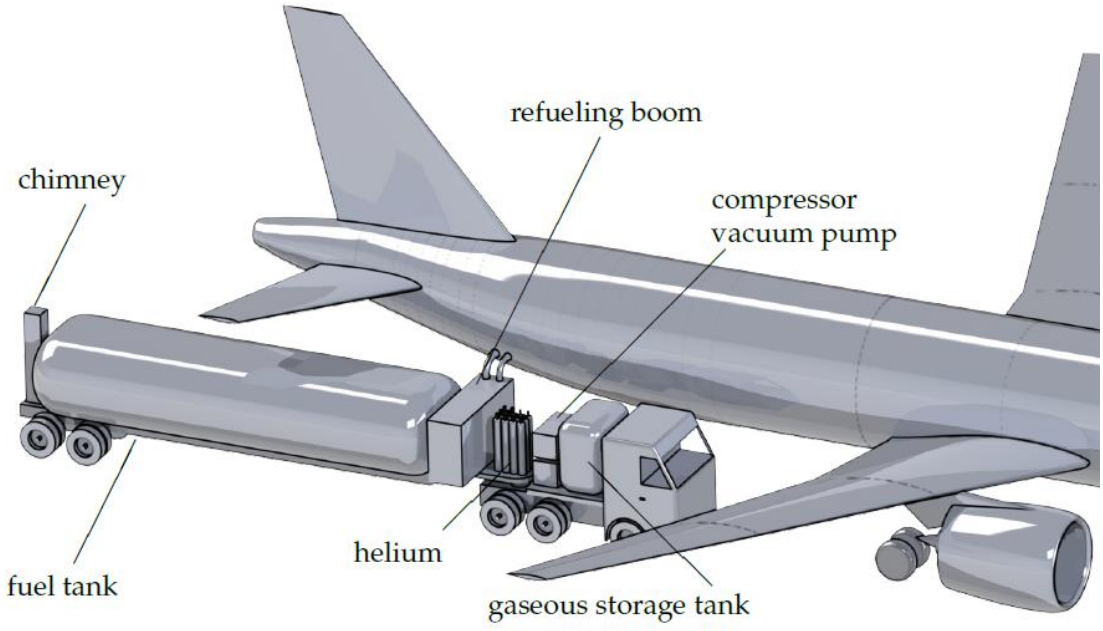

Figure 2.6: Representation of a 70 m^3 LH_2 capacity refueling truck equipped with a gaseous storage tank for boil-off gases (Mangold et al., 2022). [Open Access]

2.4.2.2. LH_2 pipeline and hydrant distribution

As mentioned above, refueling trucks will no longer be a feasible distribution method once hydrogen demand is completely established at large airports. Therefore, a liquid hydrogen pipeline and hydrant system will be the best option for distributing large fuel volumes from the storage farm to each aircraft stand. However, LH_2 pipeline distribution facilities are not expected to be deployed at large airports before 2040 or 2045 (Postma-Kurlanc et al., 2022).

This distribution method involves a huge investment compared to tankers, and a less flexible configuration. Already existing kerosene pipeline facilities cannot be adapted to LH_2 use. Therefore, a vacuum jacket pipeline system must be installed under the airport apron in a trench. This trench must be large enough to allow maintenance and inspection work and open on the top, avoiding H_2 from accumulating in case of leakage (Postma-Kurlanc et al., 2022). Building the distribution pipeline on the surface of the airport, rather than buried in a trench, is not advisable as the installation is more exposed and could even constitute an obstacle to the mobility of the ground assistance vehicles (Brewer, 1976).

Pipeline distribution technique reduces traffic on the apron, increasing safety. In addition, larger volumes of LH_2 can be delivered without repeated connection and disconnection. This results in faster aircraft refueling and turnaround times (Hoelzen et al., 2022; Mangold et al., 2022). On the contrary, the construction of this facility may disrupt the normal operation of the airport and is likely to clash with already installed utilities, leading to the redesign of facilities and high costs (Postma-Kurlanc et al., 2022). Another disadvantage is the complexity of the installation, as controlling LH_2 pressure, vacuum and leakage along the whole system will be challenging. Thus, monitoring methods and sensors will be critical for the right operation of the facility (Postma-Kurlanc et al., 2022).

As mentioned in section 2.4.1, LH_2 can be transferred through the pipeline by two different techniques. The first consists of generating a pressure differential between the storage farm tank and the destination vessel. This pressure differential is achieved by pressurizing the initial storage tank, using hydrogen itself as a pressurant. Part of the liquid is removed from the tank and allowed to vaporize, increasing in volume according to a ratio of 1:845 (Postma-Kurlanc et al., 2022). Then, the H_2 gas is introduced back into the tank, and as it warms faster than the liquid does, the gas expands applying pressure to the liquid. Once the required pressure within the tank is reached, an outlet valve is opened allowing LH_2 flow to the receiving tank. The second transfer option uses a cryogenic pump to generate the LH_2 flow from the storage farm to each aircraft stand. However, both feeding systems require a pressurization gas system to avoid a pressure drop in the tank due to the displaced fuel (Mangold et al., 2022).

Authors like Brewer (1976) consider active pumping more appropriate than a pressurized-tank feeding system as the latter generates more boil-off losses related to the pressurization and depressurization cycle of the tank. Moreover, using a feeding pump system allows to work with low pressure in the storage tank, which increases safety and can reduce tank costs. On the contrary, active pumping is more complex, which reduces reliability (Brewer, 1976). Thus, redundant pumps must be installed, meaning a significant investment that can overcome pressurized-tank savings. Lastly, it should be noted that pump work adds heat to the LH_2, consequently contributing to boiling. This is the reason why some authors recommend minimizing the use of pumps and prefer relying on pressure differential techniques (Postma-Kurlanc et al., 2022).

To avoid LH_2 two-phase flow in the primary distribution pipeline, the trench must be equipped with a parallel recovery pipe for boil-off gases. In addition, a spare pipeline should be installed for redundancy. This spare pipeline will work in case of failure or maintenance of the main pipeline and as a backup to meet higher demands (Brewer, 1976; Hoelzen et al., 2022). As in storage tanks, vacuum jacket pipelines, consisting of an inner pipe containing the cryogenic fluid surrounded by an evacuated outer jacket, are used to minimize heat transfer, and prevent LH_2 from boiling. Integrating boil-off gases within an outer layer of the primary pipeline could also be possible (Postma-Kurlanc et al., 2022). This would help to reduce heat ingress to the pipe's central core at the cost of increasing the total diameter. As mentioned previously boil-offs can be re-liquefied at the storage farm or used to power hydrogen ground support vehicles and airport facilities.

Some authors consider a pipeline loop configuration in which LH_2 constantly flows the best solution (Brewer, 1976; Hoelzen et al., 2022). This circular design keeps the required cryogenic temperatures inside the pipe and reduces BO related to cooling down during inactive or low-demand periods. The flow is pumped from the storage farm to the aircraft stands and received back in another tank at the end of the loop. On the contrary, this concept substantially increases the length of the facility, resulting in higher installation costs and a negative impact on boil-off (Postma-Kurlanc et al., 2022).

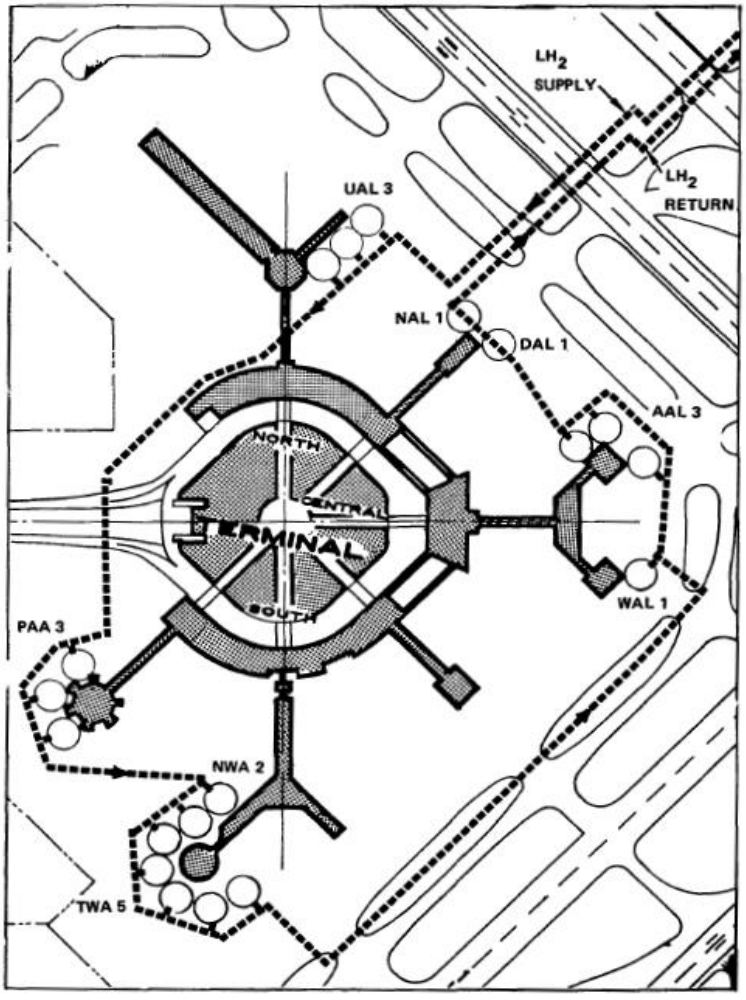

Figure 2.7: Layout of the LH_2 loop distribution system Brewer (1976) proposed at the San Francisco airport for supplying 19 aircraft stands.

The pipeline distribution system requires a hydrant pit to be located at each aircraft stand. Then, a mobile dispenser unit connects the pipeline and the aircraft tank through each hydrant as shown in Figure 2.8 The dispenser has an articulated arm that allows refueling through a flexible vacuum jacket hose. As the figure shows, a GH_2 vent hose collects boil-off gases from the aircraft tank and recirculates them to the recovery pipeline. Last, the dispenser truck is also equipped with a vacuum pump to ensure thermal insulation and typically high-pressure helium bottles to purge the hoses before and after refueling. It should be considered that a large fleet of mobile dispenser units could result in heavy traffic on the airport apron, decreasing safety and requiring vast space.

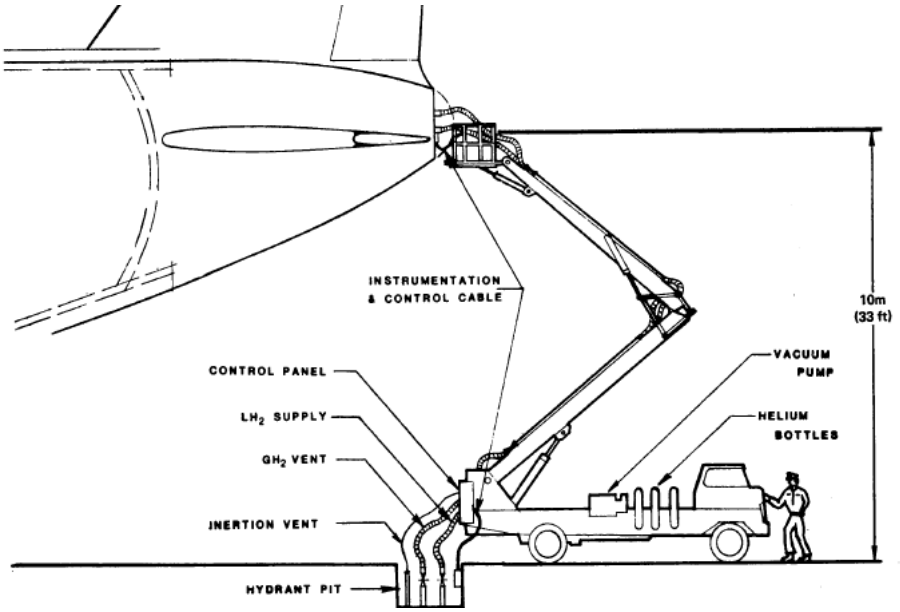

Figure 2.8: Schematic drawing of a mobile dispenser unit during aircraft refuelling (Brewer, 1976).

One of the main challenges of the described LH_2 pipeline distribution system, especially when using pressure differential feeding, is controlling pressure at each hydrant when various aircraft are being simultaneously refueled (Postma-Kurlanc et al., 2022). A potential alternative to ease achieving the required refueling pressure at each stand is installing individual pipelines from the storage farm to each stand. However, this configuration would enormously increase costs and maintenance work. Therefore, the solution proposed is building just one backbone distribution pipeline branching to each stand and locating a transfer or intermediate tank at each aircraft stand. This transfer tank can be built under or above ground. The former option is likely more expensive and less flexible as replacing the tank would be more complex. However, burying the tank minimizes space intrusion on the stand and reduces pipework length as the tank can be placed closer to the aircraft than an aboveground design. In addition, safety is increased by locating the tank underground.

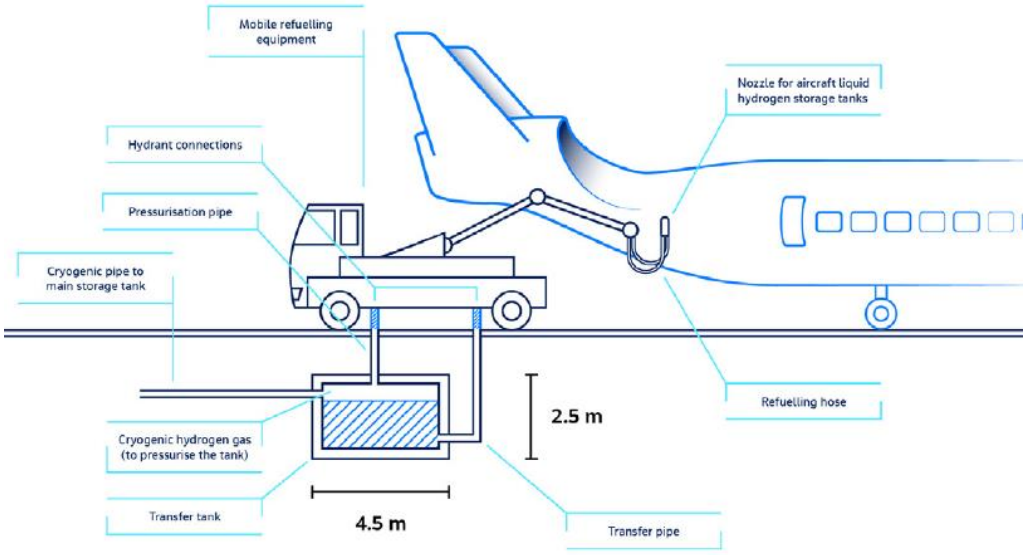

Figure 2.9: Aircraft refueling from an underground transfer tank. Adapted from Postma-Kurlanc et al.(2022).

Figure 2.9 explains how the transfer tank concept works during aircraft refueling. As seen in the figure, a mobile dispenser unit is again needed to connect the aircraft tank with the transfer tank. In this configuration, the transfer tank is pressurized, and refueling is carried out by pressure differential with the aircraft tank. Therefore, boil-off gases produced during refueling can be reintroduced in the transfer tank and used to maintain the required pressure differential.

Lastly, it should be noted that the distance between the storage farm and the aircraft stands is a critical factor in the choice of distribution system. As the distribution pipeline length increases, the higher the investment costs and the more complex the system. Furthermore, as some authors claim and will be discussed in this thesis, increasing the pipeline length leads to larger boil-off (Hoelzen et al., 2022). Comparing different authors, the average distribution length ranges from 2,000 to 3,000 meters (Hoelzen et al., 2022; Mangold et al., 2022). These values are also considered in this thesis as reasonable distances. Regarding loop distribution, the total pipeline length in Brewer's (1976) work is 6,700 meters.

2.4.3. Aircraft refueling

The last step in the LH_2 delivery chain to the aircraft is refueling. It is a critical operation that directly affects the turnaround times. One of the challenges of LH_2 aviation is to achieve the same or even shorter turnaround times than kerosene (Mangold et al., 2022). Some details have been introduced in the previous section as refueling is closely linked to distribution. Both distribution options share the basics of refueling, which is composed of five consecutive processes: docking maneuver, connecting and purging, chill-down and recovery, actual refueling mass flow, and lastly, disconnecting (Mangold et al., 2022).

1) Docking maneuver. It starts with positioning the ground vehicle delivering LH_2. This is followed by coupling the refueling hose with the aircraft tank. Due to the

lower density of LH_2 compared to kerosene, the refueling hose must be larger in diameter, making it heavier and impossible to handle by one person. In addition, manual handling of a cryogenic hose can be dangerous. Thus, the optimal solution is coupling the hose through a semi- or full-automated robotic arm located in the group vehicle (tanker or dispenser unit) (Postma-Kurlanc et al., 2022).

2) Connecting and purging. Purging is not required when refueling with kerosene. As introduced in section 2.4.2.1, no foreign gases or particles can enter the aircraft tank and fuel system as they may create explosive atmospheres. The Johnston coupling is the most used method and consists of repeated cycles of alternating vacuuming and pressurization with an inert gas, generally helium (Hoelzen et al., 2022; Mangold et al., 2022). After these cycles, foreign substances are expulsed, and the required contamination levels are met.

3) Chill-down and recovery. The temperature in the hose and tank walls must reach the boiling point of LH_2 during refueling. A reduced LH_2 mass flow is introduced to avoid large thermal stresses while facilities are cooled down. Great part of this reduced mass flow vaporizes leading to a two-phase flow. The chill-down is completed once a vapor-free flow is obtained in the hose (Mangold et al., 2022). The resulting boil-off gases must be recovered to reduce aircraft tank pressure, which would affect the pump performance, and to increase the process efficiency. Thus, two hoses must be coupled to the aircraft tank, one for LH_2 supply and the other for recovering the boil-offs and recirculating them to the distribution system.

4) Actual refueling mass flow. Once cryogenic temperature and single-phase flow are reached, actual refueling starts. Compared with kerosene, Mangold et al. (2022) claim that the equivalent energy rate required to maintain turnaround times must be 2,100 MJ/s. Translated to mass, the required mass flow is about 17.5 kg/s of LH_2. Other authors have reached similar conclusions (Boeing, 1976; Brewer, 1976). However, at the moment there is no consensus on the refueling flow and a wide range of flow rates has been proposed (Lopez, 2022). the LH_2 refueling flow is unclear. Furthermore, some limitations in the fluid speed must be respected (Mangold et al., 2022).

5) Disconnecting. Two options for disconnecting are possible. On the one hand, the Johnston disconnect method is fully developed and would be the simplest to implement (Mangold et al., 2022). On the other hand, a clean break disconnect is being developed. This technique excludes purging with consequent savings in time and money (Hoelzen et al., 2022).

3. Methodology

As introduced above, one of the main bottlenecks for hydrogen in aviation is airport distribution. To that end, this thesis aims to introduce a simplified approach for rapidly assessing LH_2-pipeline based distribution systems. The main characteristic studied is boil-off, which directly relates to efficiency losses along the LH_2-chain. Thus, first, the chosen LH_2 distribution system is described, and the study's boundaries are set. Then, components required in the distribution facility and critical factors affecting boil-off are identified. High uncertainties due to the long-term expected arrival of the technology and scarce reliable data hinder a more comprehensive analysis. Lastly, assumptions and equations used to build the mathematical model are presented.

3.1. Description of the analyzed LH_2 distribution system

As mentioned in section 2.4.2.1, pipeline distribution of LH2 becomes more economical than tankers when LH_2 demand is high (a threshold value of 342 tons/day has been estimated by Hoelzen et al. (2022), for example). Therefore, a hypothetic airport with a considerable LH_2 demand as could be expected for hubs beyond 2050 in case significant fleet penetration of hydrogen aircraft can be achieved is considered in the model. The distribution facility comprises a vacuum jacket backbone pipeline that delivers the fuel from the airport storage farm to a transfer tank at each aircraft stand. A cryogenic pumping group transfers the LH_2 flow from the storage tanks to the rest of the airport. From there, refueling would be carried out by a mobile dispenser unit through a pressure differential between the transfer tank and the aircraft tank.

The boil-off analysis focuses on the airport's pipeline distribution system, and the study's boundaries comprise the LH_2 path from the storage farm to the transfer tank as pedicted in Figure 3.1. Thus, BO occurring along the LH_2 supply chain to the airport and during aircraft refueling will not be studied or quantified.

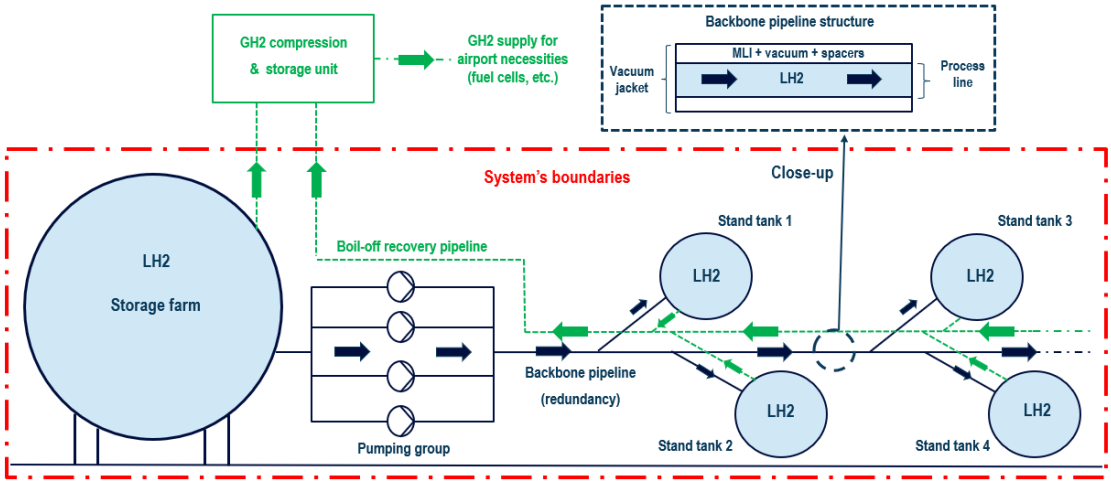

Figure 3.1: Scheme and boundaries of the analyzed LH_2 distribution model.

3.1.1. Critical factors that affect boil-off

The main factors affecting the total amount of heat added to the fuel - and with that the overall boil-off - have been identified and sorted into three main categories: airport characteristics, pipeline characteristics and pumping group characteristics. Even though factors belong to different categories, they are interrelated, and all must be considered to quantify boil-off gases. Therefore, categories are arbitrary groups that ease understanding of the model's construction. Next, each category and identified factors are introduced.

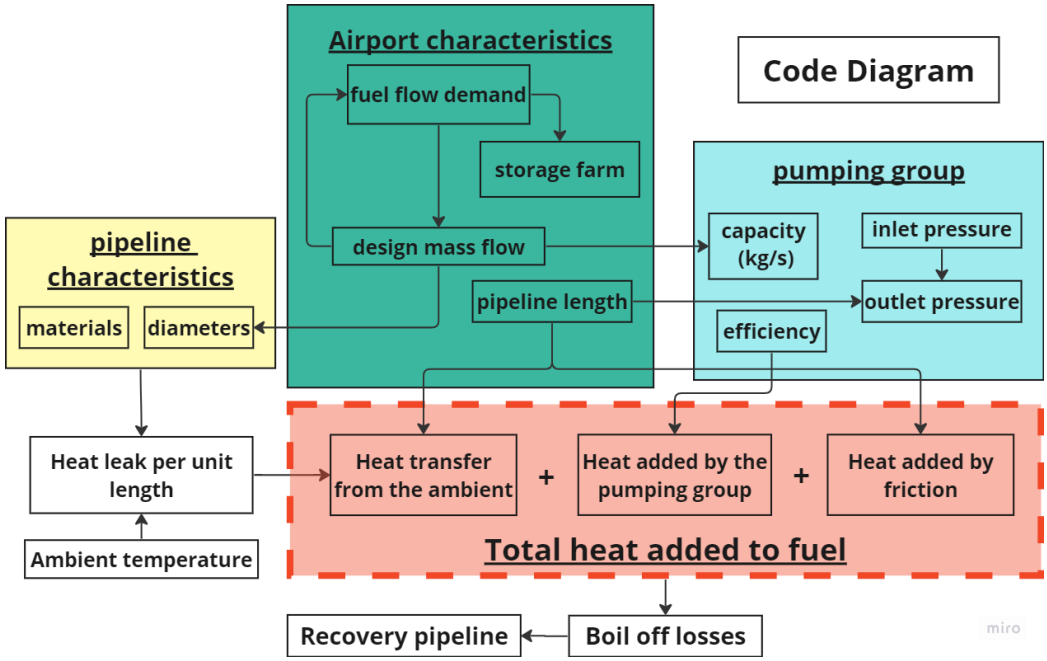

Figure 3.2: Main factors identified in the model and relationship between them.

3.1.1.1. Airport characteristics

This work does not focus on a specific existing airport. The goal is to achieve generic understanding of how could fuel boiling affect future LH_2 pipeline distribution at airports. Nevertheless, several aspects related to airport characteristics must be defined as they directly influence the sizing of the distribution facility and therefore boil-off. In most cases, average values regarding foreseen fuel consumption and facilities' size requirements are taken from literature. The most relevant factors of this category are presented.

- Airport size

  Not considering the individual hydrogen penetration of different fleets and connections offered, one can assume that the larger the airport, the greater the expected future demand for LH_2. Moreover, larger facilities would be required such as storage tanks and pipelines. Boil-off will significantly vary depending on the handled hydrogen volume and the size of the installations.

- Air traffic distribution

  The hourly arrival distribution at the airport causes LH2-demand fluctuations throughout the day. Hence, the mass flow should be adapted to best meet the

refueling needs at any given time. Distinct operation modes mean different boil-off rates.

- Location

The geographical situation of the airport sets some factors like ambient temperature or seasonal traffic fluctuations that affect heat transfer and demand requirements, respectively. The influence on boil-offs of external conditions and demand variation throughout the year is analyzed in different scenarios.

3.1.1.2. Characteristics of the distribution pipeline

As mentioned, for the distances to be covered for airport distribution a vacuum jacket pipeline is required to distribute the fuel and prevent heat ingress into the pipeline. Therefore, the pipeline's structural features, materials and size must be accurately defined.

- Structure

The distribution pipeline is typically proposed to be composed of several layers (Mital et al., 2006; Kim et al., 2022). The first layer would be an inner pipe or process line in direct contact with the cryogenic fluid. Then, an insulation material and vacuum layer would be included to minimize heat transfer. Lastly, a vacuum jacket or outer pipe surrounds the previous layers completing the vacuum chamber. Internal structural supports join the inner and outer pipes. These elements are problematic from a thermal point of view as they interrupt the insulation allowing more heat transfer.

- Materials

Due to liquid hydrogen's properties, selected materials play a key role in the design and behavior of the facility. The inner pipeline must be made of a cryogenic-resistant material capable of preventing hydrogen permeation. Austenitic steel series, 316, 316L, 316/316L, are the most commonly used materials for the manufacture of cryogenic equipment (Kim et al., 2022). In this work, the same material will be considered for both inner and outer pipelines. Moreover, multilayer insulation, MLI, introduced in section 2.4.1, and vacuum are used to insulate the LH_2 flow from outside conditions. Heat transfer will be calculated through the conduction phenomenon and the thermal conductivities of each material layer. Hence, low conductivities are vital to minimize the energy ingress per unit length, and consequent boil-offs.

- Diameter

Depending on the LH_2 airport demand and the distance, the required mass flow through the pipeline will vary. Thus, the pipeline's diameter must be adapted to the LH_2 demand requirements. There is no absolute agreement among researchers regarding which is the most suitable pipeline size. In practice, the ideal pa the diameter will be selected as a trade-off between fuel demand, investment costs and the resulting operating boil-off. Although economic aspects are not addressed in this study, oversizing the facility is not desirable as leads to unnecessary costs. In addition, the thickness of each structural layer of the pipeline will change accordingly to the pipe size, leading to different heat ingress rates per unit length. Lastly, the inner pipe diameter will affect the friction between the flow and the pipeline's walls.

- Length

This factor could also be included in the category of airport characteristics as the length of the facility will depend on the airport's size. In this thesis, an airport layout is not specified, thus, average distances extracted from the literature are analyzed (Mangold et al., 2022). Presumptively, pipeline length is expected to be one of the most critical factors in the model as the longer the pipe, the more exposed the flow is to heat transfer and the more pump work and friction forces. These aspects result in larger energy transferred to the fluid and greater boil-off (Hoelzen et al., 2022).

3.1.1.3. Characteristics of the pumping group

A cryogenic pumping group is required to transfer the LH_2 from the storage farm to each stand tank. Pumps will be located at the storage farm. Using active pumping systems adds energy to the fluid that must be considered for quantifying boil-offs. The aspects involved in the analysis are the following.

- Pump head & pump power

Pump head is the height at which a pump can raise fluid up and is measured in meters. It can be obtained from the outlet and inner pressure at the pump. In this context, the pump must provide the fluid with the mechanical energy needed to overcome friction forces and reach the destination tank at desired conditions. Thus, the pump head will be used to calculate the power required for the pumping facility. Required power directly depends on several factors of the previous two categories, such as the LH_2 mass flow, the pipeline length, and the supply pressure needed at the transfer tank.

- Pump efficiency

The pump's efficiency defines the mechanical energy provided to the fluid compared to the rated pump power. Therefore, as a solution to quantify boil-offs caused by active pumping, any inefficiencies are assumed to be fully transferred to the fluid as undesired thermal energy.

3.1.1.4. Total heat added to fuel along the distribution pipeline

As mentioned, despite high-vacuum insulation, heat ingress in the core of the pipe is unavoidable. Moreover, in this simplified description, the heat transferred to fuel along the distribution system can be originated from three causes. The first cause is the heat input from the outside due to the huge temperature gap between the ambient and the cryogenic fuel. The second cause is the pumping work. And the last aspect contributing to the heat input to LH_2 flow is the action of friction forces. The three cases are explained in more detail below, including the mathematical equations used to build the model and quantify boil-offs. In real life, there are more factors that introduce heat into the pipe core such as heat penetration through direct conductivity through the structural supports.

3.2. Construction of the model

In this section, the mathematical equations that integrate and correlate the previous identified factors within this simplified model are presented. These equations allow to size required facilities at different operating scenarios and calculate and analyze the respective influence on boil-off. To do this, some physical and technical parameters are defined as fixed values. On the contrary, other variables such as mass flow, pipe diameter and length, ambient conditions, etc., will be modified to understand how these changes affect the behavior of the distribution system regarding to fuel boiling.

3.2.1. Starting hypotheses of the model

Due to the complexity of the topic and scholars' limited knowledge a series of starting hypotheses are adopted to simplify the model and ease calculations. The list of hypotheses is the following:

1) It is assumed that LH_2 constantly flows through the pipeline. In this way, cryogenic temperature inside the inner pipe is maintained at any given time, and there is no need to consider chill-down phases.

2) The temperature of the liquid does not increase along the pipeline. The temperature remains equal and slightly below the boiling point of hydrogen, roughly 20 K.

3) Due to the proximity to the boiling point, the energy transferred to the fuel is considered latent heat. This means heat introduction causes fuel vaporization instead of increasing its temperature.

4) Liquid single-phase flow is considered in the inner pipe to simplify the behavior of the fluid and ease facility sizing. This entails (the practically not realizable) assumption of immediate evacuation of any gaseous species from the flow. In practice, the removal of gaseous species is enabled through recovery pipelines but two-phase flow will inevitably exist.

5) LH_2 is assumed as an incompressible fluid, i.e., the fuel density is considered constant. Variations of the liquid's density due to pressure and temperature changes are considered negligible within the operating window. Thus, the assumed density is about 71 kg/m^3. This value is the LH_2 density measured at 1 bar and 20.4 K.

These starting hypotheses are the basis allowing the construction of the model. While this approach does not allow quantification with high accuracy due to above described simplifications, it enables a rapid initial comparative assessment of different scenarios. It should be noted that not many examples of LH_2 pipe distribution utilities have been

realized. Therefore, publicly available information is limited, current uncertainties may be gradually clarified in the following years assuming continued development.

Apart from these hypotheses, further assumptions, which are explained below, are made during the construction of the model.

3.2.2. Mathematical equations of the model

Based on the previous hypotheses, several equations are used to characterize the generic airport requirements and quantify total heat added to the fuel along the distribution system. The equations are grouped according to each heat source identified: outside ambient, pumping work and friction forces.

3.2.2.1. Heat transfer from the outside

Heat transfer mechanisms are conduction, convection, and radiation. Convection and radiation are assumed to be negligible compared to the contribution of conductive heat transfer. Hence, heat input into the pipeline is calculated through the conduction. Conduction is the transfer of heat through a physical medium, which may be solid o fluid, from points in the medium that are at a high temperature to comparatively cooler points.

bIn the distribution pipeline, heat flux occurs from outside to inside perpendicularly to the pipeline walls. The temperature of the outer surface of the vacuum jacket is considered constant and equal to the ambient temperature. In turn, the inner surface of the inner pipeline is assumed to be at the same temperature of LH_2, roughly 20 K. Within the evacuated annulus, as there is no physical medium, the heat transferred is orders of magnitude lower compared to the transfer across the walls of the outer and inner pipelines. Hence, heat conduction in the evacuated annulus occurs through the structural supports and the MLI. In the model, radiation transfer in the vacuum is substituted by an equivalent vacuum thermal conductivity at a certain low pressure accounted for by Kim et al. (2022).

Conduction is described by Fournier's Law, which in the case of a pipeline, i.e., according to cylindrical coordinates, has the following form:

$$\frac{\mathbf{1}}{\boldsymbol{r}}\frac{\boldsymbol{\partial}}{\boldsymbol{\partial r}}\left(\boldsymbol{k}\cdot\boldsymbol{r}\frac{\boldsymbol{\partial T}}{\boldsymbol{\partial r}}\right)=\boldsymbol{\rho}\cdot\boldsymbol{Cp}\frac{\boldsymbol{\partial T}}{\boldsymbol{\partial t}} \tag{3.1}$$

where

r is the pipe radius $[m]$

k is the material thermal conductivity $[W/(m\cdot K)]$

T is temperature $[K]$

Cp is the material specific heat capacity $[J/(kg\cdot K)]$

t is time $[s]$

In this case, as the model is time-independent, the right term of Equation (3.1) is equalled to zero. Therefore, heat flow ingress per unit length of the pipeline from the outside to the LH_2, q'_{input}, can be obtained through this expression:

$$q'_{input} = {q_{input}}/{L} = \frac{T_{amb} - T_{LH2}}{\sum \frac{\ln\left(\frac{R_i}{r_i}\right)}{2\pi k_i}} \quad [W/m] \tag{3.2}$$

where q_{input} is the total heat input into the pipeline $[W]$, L is pipeline length $[m]$, and lastly, T_{amb} and T_{LH2} are the ambient and the inner pipeline temperature $[K]$, respectively. As the pipeline is composed of several layers, corresponding to different materials and thicknesses, the subindex i appearing in the formula refers to each layer's characteristics. Thickness and thermal conductivity are used to calculate each layer's linear thermal resistance, indicating the physical medium's opposition to heat flow. The larger the thermal resistance, the less heat flow is transferred across the layer. As layers are in series, the equivalent thermal resistance of the pipe wall is obtained by adding the linear thermal resistances of the layers. The resulting term appears in the denominator of Equation (3.2):

$$R'_{equiv} = \sum \frac{\ln\left(\frac{R_i}{r_i}\right)}{2\pi k_i} \quad [mK/W] \tag{3.3}$$

where R_i and r_i are each layer's outer and inner radius $[m]$, respectively.

The thickness of each layer is different and is based on previous studies that have proved a high insulation level (Kim et al., 2022).

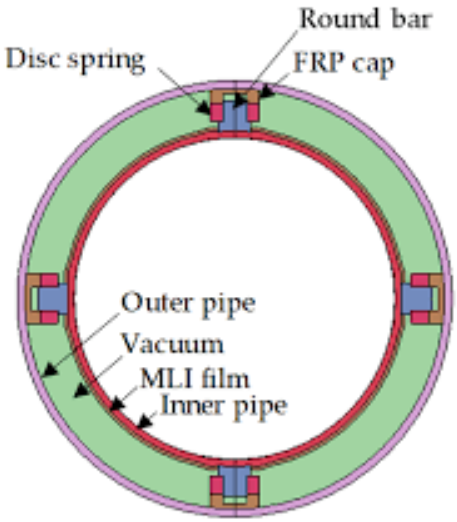

Figure 3.3 Layer structure of the vacuum jacket distribution pipeline (Kim et al., 2022).

3.2.2.2. Heat added by the pumping group

The pumping group provides energy to the fluid to transfer it from the storage farm to each aircraft stand. Most of this energy is mechanical, but some is transformed into heat according to the pump's efficiency. Heat input of the pumping system to the fluid causes boil-off. Therefore, the pumping unit must be sized according to airport requirements to quantify the boiling effect. The strategy selected to characterize the pipeline and pumps is based on Bernoulli's theorem.

- **Bernoulli's theorem**

Bernoulli's theorem describes a fluid's motion behavior along a pipeline and establishes an energy conservation equation between different points of the duct. The whole mechanical energy of the fluid is composed of several terms, which are the fluid pressure energy, the kinetic energy of the fluid, and the gravitational potential energy of elevation (García, 2016; Menon, 2005). Assuming an incompressible fluid, constant temperature, and no heat transfer between the flow and the outside, which is considered in the previous section, Bernoulli's theorem has the following appearance:

$$\frac{\boldsymbol{p}_1}{\boldsymbol{\gamma}} + \frac{\boldsymbol{v}_1^2}{2\boldsymbol{g}} + \boldsymbol{z}_1 = \frac{\boldsymbol{p}_2}{\boldsymbol{\gamma}} + \boldsymbol{z}_2 + \frac{\boldsymbol{v}_2^2}{2\boldsymbol{g}} + \boldsymbol{z}_2 \tag{3.4}$$

where

p is the fluid pressure $[Pa]$

γ is the fluid volumetric weight $[N/m^3]$

v is the fluid speed $[m/s]$

z is the height of the fluid $[m]$

g is the gravitational acceleration $\left[m/s^2\right]$

This ideal equation states that the fluid energy at any point of the duct can be described by the pressure energy, p/γ, the kinetic energy, $v^2/2g$, and the potential energy, z. Although these terms may vary along the pipeline, the total sum must be constant at any section of the pipe. The resulting terms are all measured in metres.

- **Pressure losses due to friction forces**

The contact of the fluid in motion with the inner wall of the pipeline produces friction resulting in a reduction of the fluid mechanical energy. The energy reduction is mainly appreciated as a pressure loss as the pipeline length increases. Pressure losses can be sorted into primary and secondary losses. Primary losses are due to friction in straight pipe segments and directly depend on duct length. Instead, secondary losses are caused by valves, fittings, bends or unions, which force the flow to gradually or abruptly adapt to changes in direction and the cross section or shape of the pipeline (Polizelli et al., 2003).

Bernoulli's theorem must be adjusted to consider the friction effect along the pipe. Thus, considering two points of the distribution system, one point immediately after the pumping group and the second one separated a considerable distance from the storage farm, Bernoulli's theorem adopts the following shape:

$$\frac{\boldsymbol{p_1}}{\boldsymbol{\gamma}} + \frac{\boldsymbol{v_1^2}}{\boldsymbol{2g}} + \boldsymbol{z_1} + \boldsymbol{H_P} = \frac{\boldsymbol{p_2}}{\boldsymbol{\gamma}} + \boldsymbol{z_2} + \frac{\boldsymbol{v_2^2}}{\boldsymbol{2g}} + \boldsymbol{z_2} + \boldsymbol{h_f^{1-2}} + \boldsymbol{h_{sec}^{1-2}} \tag{3.5}$$

where

H_P is the pump head provided by the pumping group $[m]$

h_f^{1-2} is the pressure drop due to primary losses between points 1 and 2 $[m]$

h_{sec}^{1-2} represents the secondary pressure losses between points 1 and 2 $[m]$

The primary losses, h_f, can be obtained by several equations, but one of the most commonly used formulas is the *Darcy-Weisbach* equation, which is only valid for turbulent flows:

$$\boldsymbol{h_f} = \boldsymbol{f} \cdot \frac{\boldsymbol{L}}{\boldsymbol{D}} \cdot \frac{\boldsymbol{v^2}}{\boldsymbol{2g}} \tag{3.6}$$

where

$_f$ is the friction factor [dimensionless]

L is the length of the pipeline $[m]$

D is the inner diameter of the pipeline $[m]$

v is the flow speed $[m/s]$

g is the gravitational acceleration $[m/s^2]$

In turn, the friction factor, $_f$, depends on the relative roughness of the material, ε/D, and the Reynolds number, Re. For turbulent flows, i.e., when $Re > 4{,}000$, the friction factor is generally calculated through the *Colebrook* equation:

$$\frac{\boldsymbol{1}}{\sqrt{\boldsymbol{f}}} = \boldsymbol{-2 \cdot \log_{10}\left(\frac{\varepsilon}{3.71 \cdot D} + \frac{2.51}{Re\sqrt{f}}\right)} \tag{3.7}$$

where

ε is the absolute roughness of pipeline, which depends on the used material $[m]$

D is the inner diameter of the pipeline $[m]$

The Reynolds number is also a dimensionless quantity that is used to characterize the flow behaviour between laminar or turbulent regime. It is obtained as follows:

$$\boldsymbol{Re = \frac{\rho \cdot v \cdot D}{\mu}} \tag{3.8}$$

where

ρ is the density of the fluid, liquid hydrogen in this case $[kg/m^3]$

v is the flow speed $[m/s]$

D is the inner diameter of the pipeline $[m]$

μ is the dynamic viscosity of the fluid $[Pa \cdot s]$

To simplify calculations, Equation (3.7) is substituted by the *Sjoen* equation, which allows to obtain the friction factor directly and provides small errors (García, 2016).

$$\boldsymbol{f = 1.325 \cdot \left[-ln\left(\frac{\varepsilon}{3.7 \cdot D} - \frac{1.963}{Re} \cdot ln\left(\left(\frac{\varepsilon}{3.7 \cdot D} \right)^{\frac{10}{9}} + \frac{6.9}{Re} \right) \right) \right]^{-2}} \tag{3.9}$$

Regarding the secondary pressure losses, as the layout of the distribution system is unknown, the resulting pressure drop cannot be calculated accurately. Therefore, secondary losses in this work are estimated as a 5% of the primary pressure losses.

- **Sizing of the pumping group**

The task of the pumping group is delivering the fuel at each aircraft stand at the required mass flow and pressure conditions. To achieve this, the pumps must provide the fluid with enough energy to travel along the pipeline overcoming the pipe routing and friction forces that hinder flow. The energy provided by the pumping group at the storage farm is defined by the term H_P of Equation (3.5), which represents the equivalent head added to the fluid and is measured in meters.

The pump head, H_P, can be calculated as the difference between the outlet and inlet pressure at the pumping group, also known as discharge and suction pressure, respectively. As shown in Equation (3.10), both pressure terms are divided by the volumetric weight of LH_2, resulting from multiplying LH_2 density by the gravity constant. In this way, pressure originally measured in *Pascal* is transformed into an equivalent height.

$$\boldsymbol{H_P = \frac{p_{discharge}}{\gamma} - \frac{p_{suction}}{\gamma}} \tag{3.10}$$

In turn, discharge and suction pressures must be defined through the adjusted *Bernoulli's theorem*, Equation (3.5). First, the reasoning to obtain the discharge pressure is introduced. As previous cases, two points of the pipeline are analyzed. The first point is the outlet of the pumping group whereas the second one is the most distant aircraft stand, which represents the most unfavorable delivery scenario. Thus, the discharge pressure must be large enough to ensure minimum supply pressure conditions at the furthest transfer tank. If the discharge pressure meets the pressure level in the worst case, pressure and flow requirements in the closer remaining aircraft tanks will be satisfied.

$$\boldsymbol{\frac{p_{discharge}}{\gamma} = \frac{p_{min}^{+distant}}{\gamma} + (z_{stand} - z_{pump}) + \left(\frac{v_{stand}^2}{2g} - \frac{v_{discharge}^2}{2g}\right) + h_f^{1-2} + h_{sec}^{1-2}} \tag{3.11}$$

Considering that both points are at the same elevation, potential terms can be cancelled. In addition, diameter and therefore flow speed is considered constant along the whole pipe. Therefore, kinetic terms can also be deleted, and Equation (3.11) is simplified to:

$$\boldsymbol{\frac{p_{discharge}}{\gamma} = \frac{p_{min}^{+distant}}{\gamma} + h_f^{1-2} + h_{sec}^{1-2}} \tag{3.12}$$

where

$p_{discharge}/\gamma$ is the outlet pressure at the pumping group $[m]$

$p_{min}^{+distant}/\gamma$ is the minimum pressure supplied at the most distant transfer tank $[m]$

h_f^{1-2} are the total primary pressure losses between the pump and the transfer tank $[m]$

h_{sec}^{1-2} are the total secondary pressure losses along the analyzed pipe segment $[m]$

When calculating the suction pressure, a similar strategy is followed, but in this case the analyzed pipe segment is located between the storage tank and the inlet of the pumping group. According to Brewer (1976), pumps must be close coupled to the storage farm tank to minimize heat ingress into the pump suction piping and avoid the presence of two-phase flow. As distance between the tank and the pumping group is very short, pressure drop will be low. The same assumptions are considered about elevation and flow speed, resulting in the following expression:

$$\frac{\boldsymbol{p_{suction}}}{\boldsymbol{\gamma}} = \frac{\boldsymbol{p_{storage}}}{\boldsymbol{\gamma}} - \boldsymbol{h_f^{1'-2'}} - \boldsymbol{h_{sec}^{1'-2'}} \tag{3.13}$$

where

$p_{suction}/\gamma$ is the inlet pressure at the pumping group $[m]$

$p_{storage}/\gamma$ is the outlet pressure at the storage farm tank $[m]$

$h_f^{1'-2'}$ are the primary pressure losses between the storage farm tank and the pump $[m]$

$h_{sec}^{1'-2'}$ are the secondary pressure losses along the analyzed pipe segment $[m]$

In this case, pressure losses are expected to be low or even neglected as the distance between the storage tank and the pumping system is very short. Consequently, substituting the previous terms in Equation (3.10), the expression to calculate the pump head can be reformulated:

$$\boldsymbol{H_P} = \frac{\boldsymbol{p_{discharge}}}{\boldsymbol{\gamma}} - \frac{\boldsymbol{p_{suction}}}{\boldsymbol{\gamma}} = \frac{\boldsymbol{p_{min}^{+distant}}}{\boldsymbol{\gamma}} - \frac{\boldsymbol{p_{storage}}}{\boldsymbol{\gamma}} + \boldsymbol{h_f^{1-2}} + \boldsymbol{h_{sec}^{1-2}} + \boldsymbol{h_f^{1'-2'}} + \boldsymbol{h_{sec}^{1'-2'}} \tag{3.14}$$

Once the pump head is known, the mechanical energy provided to the mass flow can be obtained. As the pump performance is limited by the mechanical efficiency, the power requirements can be sized as follows (García, 2016):

$$\boldsymbol{P_{pump}} = \frac{\dot{\boldsymbol{m}} \cdot \boldsymbol{g} \cdot \boldsymbol{H_P}}{\boldsymbol{\eta}} \tag{3.15}$$

where

P_{pump} is the power of the pumping system $[W]$

$\dot{m}$ is the LH_2 mass flow distributed through the pipe $[kg/s]$

g is the gravity constant $[m/s^2]$ and η is the pump efficiency

Thus, as mentioned in section 3.1.1.3, the power and the pump efficiency are used to calculate the heat added to the fluid by the pump work, q_{pump}. The remaining energy

that the pump cannot provide to the fluid as mechanical energy is assumed to be fully transferred as thermal energy to the LH_2 and is calculate through Equation (3.16).

$$\boldsymbol{q_{pump}} = \boldsymbol{P_{pump}} \cdot (1 - \boldsymbol{\eta}) \ [\boldsymbol{W}] \tag{3.16}$$

An electric motor is required to drive the pump. Considering that the motor has an electrical efficiency, η_{el}, of 0.9 and applying a safety factor of 1.1, both values taken from García (2016), the minimum power of the electric motor is calculated.

$$\boldsymbol{P_{el}} = 1.1 \cdot \frac{\boldsymbol{P_{pump}}}{\boldsymbol{\eta_{el}}} \ [\boldsymbol{W}] \tag{3.17}$$

3.2.2.3. Heat added by friction

Lastly, the strategy to quantify the heat added by friction to LH_2 within the duct is introduced. Friction is originated from the interaction between the fluid in movement and the pipe inner wall. Friction forces are opposed to flow and lead to a reduction of the total fluid mechanical energy. The lost energy is transformed into thermal energy and, in most cases, dissipates through the walls of the duct. However, considering cryogenic liquid hydrogen, the generated heat is unlikely to dissipate and will drive to flow vaporization and boil-off gases.

Based on the adopted hypotheses, no clear methods to quantify the heat generation by friction have been found in the specialized literature. Therefore, in this thesis, friction heat is estimated from a hypothetical situation. As the most direct evidence of the friction effects is the resulting pressure loss in the fluid along the pipeline, pressure losses are transformed into undesired heat. To do this, the pressure drop, resulting from both primary and secondary pressure losses, at the analyzed duct is assumed to be the pump head of a hypothetical pumping group that only provides thermal energy to the fluid. Thus, Equation (3.15) can be used to quantify the horsepower of this fictitious pump, $\boldsymbol{P_{pump}^{friction}}$. Considering that the whole reduction of the fluid mechanical energy due to friction is directly transformed to heat, the estimated thermal energy added to the LH_2 flow, $\boldsymbol{q_{friction}}$, is obtained.

$$\boldsymbol{P_{pump}^{friction}} = \dot{\boldsymbol{m}} \cdot \boldsymbol{g} \cdot \boldsymbol{H_{pressuredrop}} = \boldsymbol{q_{friction}} \ [\boldsymbol{W}] \tag{3.18}$$

where

$\boldsymbol{H_{pressure\ drop}}$ are the total pressure losses due to friction at the pipeline $[m]$

Although this strategy is an approximation, it has been considered the optimum form to estimate heat added to the LH_2 mass flow respecting the hypothesis described in section 3.2.1.

3.2.2.4. Calculation of the boil-off along the distribution pipeline

The three heat contributing sources, outside ingress, pump, and friction heat, have been identified and quantified according to the airport's distribution requirements. As mentioned in hypothesis 3) of section 3.2.1, thermal energy added to the LH_2 flow is considered latent heat. Hence, the fluid temperature does not rise, and heat is entirely focused on the change of state from liquid to gas. Therefore, the resulting boil-off gases along the distribution system can be easily calculated from the total heat added to the LH_2 flow, $\boldsymbol{q_{total}}$ and the LH_2 latent heat of vaporization, $\Delta \boldsymbol{H_{vap}^{LH2}}$. The latter indicates the required supplied energy to vaporize one kilogram of liquid hydrogen at constant temperature. The following equations show how the total BO are obtained:

$$\boldsymbol{q_{total}} = \boldsymbol{\dot{m}_{total\,BO}} \cdot \Delta \boldsymbol{H_{vap}^{LH2}} \tag{3.18}$$

$$\boldsymbol{q_{total}} = \boldsymbol{q_{input}} + \boldsymbol{q_{pump}} + \boldsymbol{q_{friction}} \tag{3.19}$$

$$\boldsymbol{\dot{m}_{total\,BO}} = \boldsymbol{\dot{m}_{input\,BO}} + \boldsymbol{\dot{m}_{pump\,BO}} + \boldsymbol{\dot{m}_{friction\,BO}} \tag{3.20}$$

3.2.3. Parameters of the base case model

A base airport scenario must be defined hereafter to allow LH_2 boiling analysis along the pipeline distribution system. Thus, a starting series of parameters is fixed to establish the base model. Further, the impact of certain parameters on boil-off is analyzed. In addition, results will be compared, and the configuration selected will be discussed.

As a reasonable threshold for implementing a pipeline system, authors have found a consumption of 342 tons per day (Hoelzen et al., 2022). Based on that and following the argumentation of Lopez (2022), the peak demand is assumed to be 615 tons of LH_2 per day. This peak demand is associated with the busiest month of the year. Air traffic seasonal fluctuation is a very common phenomenon at airports and facilities must be sized to meet fuel requirements under the most demanding circumstances. In many cases, air traffic fluctuation is directly related to geographical situation of the airport and the weather. In this thesis, Munich is chosen as the base case location for its proximity and intense air traffic. Therefore, Munich's airport weather and air traffic variations throughout the year are taken as a reference. In 2019, the busiest period in Munich's airport was September (Munich Airport, 2019b); thus, the peak demand is associated to this month and the average temperature of September is considered for heat transfer estimates.

Another important parameter is the mass flow in the distribution pipeline, which in the base case is considered constant during the entire day. Dividing the LH_2 consumption by the total number of seconds in a day and multiplying by 1.05 as a safety factor to offset possible losses, a continuous mass flow of 7.47 kg/s is obtained. In reality, as aircraft arrivals are not homogenous throughout the day, the mass flow is more likely to be variable.

Continuing with the pipeline characteristics assumed herein, the vacuum jacket pipeline's materials are 316 stainless steel for both inner and outer pipes and multilayer insulation accompanied by a vacuum annulus in between. Structural supports are not directly considered in the model. Thermal conductivities and thicknesses of each structural layer are constant in the whole analysis and are extracted from a previous experimental work (Kim et al., 2022). Regarding the length of the duct, an average length of 2,000 meters is assumed for the base case, which is in line with the literature (Hoelzen et al., 2022; Mangold et al., 2022). The pipe length between the storage farm tank and the pumping group is fixed at 1.5 meters, as these elements must be in close proximity.

Table 3.1: Thermal properties and thicknesses of the pipe's layers (Kim et al., 2022).

Layers	***Materials***	***Conductivity, k*** (W/mK)	***Thickness, t*** (mm)
Inner pipe	316 stainless steel	14.6	3.44
Insulation	MLI	0.000135	1.82
Evacuated annulus	Vacuum (≤1 mbar)	0.0001	19.43
Outer pipe	316 stainless steel	14.6	4.19

Next, the parameters defining the pumping group in the base case are introduced. As mentioned in section 3.2.2.2, the storage farm pressure and the transfer tank pressure are critical to calculate the pump head and power requirements. The storage farm pressure is fixed at 1.1 bar as it must be above atmospheric pressure to avoid air ingress into the tank (Boeing, 1976). Then, the supply pressure at the transfer or intermediate tank must be at least 1.5 bar. It should be remembered that aircraft are refueled by differential pressure between the intermediate and the airplane tank. Therefore, supplying the LH_2 flow to the transfer tank at a certain pressure level facilitates the subsequent refueling process.

The main parameters involved in the model are shown in Table 3.2. Some of them are fixed whereas others are varied to analyze their influence on boil-off. The current values of the variable parameters are for the base case and will change when considering other scenarios. The value of the pipeline diameter is not specified in advance as there is no full agreement among scholars on the most suitable pipe size. Therefore, it is discussed below which diameter minimizes the boil-off gases for the base case.

Table 3.2: Main parameters in the model, possible types (fixed or variable) and values of the base case.

Parameters	***Type***	***Value/Reference***
LH_2 daily consumption	Variable	615 tons
LH_2 mass flow	Variable	7.47 kg/s
Location	Fixed	Munich, Germany
Average ambient temperature	Variable	14 ºC
LH_2 inner temperature	Fixed	20.4 K
Pipe thermal properties	Fixed	Table 3.1
Pipe absolute roughness	Fixed	0.00008 m (Mangold et al., 2022)
Distance farm-pump	Fixed	1.5 m
Pipe diameter	Fixed	Discussed below
Pipe length	Variable	2,000 m
Storage farm pressure	Fixed	1.1 bar
Transfer tank pressure	Variable	1.5 bar
Pump efficiency	Variable	0.73
LH_2 density	Fixed	71 kg/m^3
LH_2 latent heat of vaporisation	Fixed	447 kJ/kg
LH_2 dynamic viscosity	Fixed	0.000013 Pa·s (StackExchange, 2021)

4. Results and Discussion

This chapter shows the results obtained in this study applying the simplified modeling approach discussed int Chapter 3. First, the optimal diameter of the distribution pipe for the base case is studied. Then, once the pipe size is chosen, average operating conditions are defined and the performance of the distribution system is analyzed. The boil-off rate along the distribution pipe is calculated and the potential use of the energy contained in the boil-off gases is discussed. Finally, a parametric analysis is performed in which it is studied how the previous results change if certain parameters of the system are modified. The parameters analyzed are the insulation correction factor, the ambient temperature, the pipe length, the mass flow, the pump efficiency and the supply pressure at the transfer tank.

4.1. Base case scenario

4.1.1. Study of the pipeline diameter

It is not obvious which is the most appropriate pipeline diameter for the described scenario. In addition, a wide range is reported in literature. Some examples are presented:

- In the work of Brewer (1976), a similar LH_2 consumption is considered, 731.4 tons per day. The author states that the pipe diameter must be greater than 10 inches (254 mm) to reduce friction. However, the mass flow that Brewer considers is almost twice, approximately 13.5 kg/s, the base case mass flow of this study

- Other authors suggest that a mid to large airports would require a pipe diameter of 20 inches, approximately 500 mm (Postma-Kurlanc et al., 2022).

- Finally, a diameter of 28 inches (714 mm) and a mass flow of 93.5 kg/s is considered by Lopez (2022) for the LH_2 demand assumed in this thesis, 615 tons.

Therefore, to get a first approximation of the most suitable pipe diameter in the base case, five different diameters are compared. As mass flow is assumed constant during the whole day, 7.47 kg/s, the duct diameter can be set by imposing different flow speeds in the pipeline according to Equation 4.1.

$$\dot{\boldsymbol{m}} = \boldsymbol{\rho} \cdot \boldsymbol{A} \cdot \boldsymbol{v} \tag{4.1}$$

where

$\dot{m}$ is the mass flow $[kg/s]$
ρ is LH_2 density $[kg/m^3]$
A is the duct section $[m^2]$
$\boldsymbol{v}$ is the flow speed $[m/s]$

The fluid speed depends on the flow rate and the cross-section of the pipeline. Thus, at equal mass flow, the lower the flow speed, the larger the diameter, and vice versa. To guarantee a correct supply and avoid safety concerns, the LH_2 flow speed in long pipes must comply with some restrictions (Mangold et al., 2022):

$$\mathbf{1\ m/s \leq v \leq 8\ m/s} \tag{4.2}$$

$$\mathbf{v \cdot d \leq 2.35\ m^2/s} \tag{4.3}$$

where d is the inner diameter of the inner pipe $[m]$. Thus, the system operation is analyzed under five different flow speeds: 1, 2, 4, 6 and 8 m/s.

First, pipeline diameters corresponding to the previous fluid speeds are calculated and rounded to an integer value measured in inches. Results are expressed in inches to ease references and comparison along the thesis. These diameters are defined as the outer diameter of the inner pipeline. Therefore, fluid speed must be recalculated considering the pipeline's inner diameter, which can be obtained through the specified pipe thickness in Table 3.1. The results are shown in the following table.

Table 4.1: Diameter of the inner pipe depending on the fluid speed under the base case mass flow, 7.47 kg/s.

$\boldsymbol{Flow\ speed}$ $(\boldsymbol{m/s})$	$\boldsymbol{First\ diameter}$ $(\boldsymbol{in})$	$\boldsymbol{Rounded\ diameter}$ $(\boldsymbol{in})$	$\boldsymbol{Corrected\ flow\ speed}$ $(\boldsymbol{m/s})$
8	5.10	5.5	7.60
6	5.88	6	6.33
4	7.21	7	4.59
2	10.19	10	2.19
1	14.41	14	1.10

The calculations are made with the values of the two right columns of Table 4.1. It should be noted that the smallest diameter is set at 5.5 inches instead of 5 to avoid exceeding the maximum fluid speed limit, which is 8 m/s. The same reasoning applies to the largest diameter, which is rounded to 14 inches to respect the minimum speed value. Thus, it can be concluded from Table 4.1 that considering the base case mass flow, 7.47 kg/s, the pipe diameter of the facility must range between 5.5 and 14 inches. If the mass flow changes, the range of diameters will change. The larger the mass flow, the greater the average diameter, and vice versa.

According to the thicknesses specified in section 3.2.3, the diameters of the structural layers of the previous pipelines are shown in Table 4.2. The values represent the outer diameters of each layer.

Table 4.2: Outer diameters of each structural layer for the different pipe sizes.

$\boldsymbol{Pipe\ size}$ $(\boldsymbol{in})$	$\boldsymbol{D_{inner\ pipe}}$ $(\boldsymbol{mm})$	$\boldsymbol{D_{MLI}}$ $(\boldsymbol{mm})$	$\boldsymbol{D_{vacuum}}$ $(\boldsymbol{mm})$	$\boldsymbol{D_{outer\ pipe}}$ $(\boldsymbol{mm})$
5.5	139.7	143.34	182.2	190.58
6	152.4	156.04	194.9	203.28

7	177.8	181.44	220.3	228.68
10	254	257.64	296.5	304.88
14	355.6	359.24	398.1	406.48

Once the pipelines' size and structure are defined, the total heat added to the LH_2 flow is analyzed from three different points of view: heat input from the outside, heat added by the pump and heat added by friction.

4.1.1.1. Analysis of the heat input from the outside

The heat transfer from the ambient to the pipe core directly depends on the outer temperature at the airport and the equivalent thermal resistance of each pipe size. As the temperature inside the pipeline is constant, 20.4 K, because the fluid is assumed to keep constantly flowing, the heat input per distance from the outside is independent of the mass flow.

The average temperature in Munich in September, 287 K, is chosen for the base case. First, the individual linear thermal resistances and the equivalent linear thermal resistances of each pipe are calculated through Equation (3.3).

Table 4.3: Linear thermal resistances of each layer and the equivalent resistances, R'_{equiv}, for the different pipe sizes.

$\boldsymbol{Pipe\ size}$ $(\boldsymbol{in})$	$\boldsymbol{R'_{inner\ pipe}}$ $(\boldsymbol{mK/W})$	$\boldsymbol{R'_{MLI}}$ $(\boldsymbol{mK/W})$	$\boldsymbol{R'_{vacuum}}$ $(\boldsymbol{mK/W})$	$\boldsymbol{R'_{outer\ pipe}}$ $(\boldsymbol{mK/W})$	$\boldsymbol{R'_{equiv}}$ $(\boldsymbol{mK/W})$
5.5	4.96E-04	30.32	381.79	4.42E-04	412.12
6	4.54E-04	27.83	353.92	4.14E-04	381.75
7	3.88E-04	23.89	308.86	3.67E-04	332.76
10	2.70E-04	16.77	223.59	2.74E-04	240.36
14	1.92E-04	12.01	163.47	2.05E-04	175.48

Several interesting observations can be highlighted in Table 4.3. First, regarding structural layers, the thermal resistances of inner and outer pipes are negligible compared to those of the MLI and the vacuum annulus. Particularly, the contribution of vacuum to the equivalent thermal resistance of each pipe is above 92%. Moreover, it is observed that increasing the duct size reduces the equivalent thermal resistance as the heat transfer surface increases. Therefore, the larger the distribution pipeline, the lower the opposition to heat ingress in the pipe core.

The resulting heat inputs per pipe size are presented in Table 4.4. The third column shows the heat ingress per unit length, $\boldsymbol{q'_{input}}$, obtained via Equation (3.2). The column on the right shows the total heat transferred from the outside along the pipeline, $\boldsymbol{q'_{input}}$,considering a pipeline with an average length of 2,000 meters. These values can be used directly to calculate the boil-off in each case.

Table 4.4: Heat input per unit length, q'_{input}, and total heat ingress along the distribution facility, q_{input}, in the base case for the different pipe sizes.

$\boldsymbol{Pipe\ size}$ $(\boldsymbol{in})$	$\boldsymbol{R'_{equiv}}$ $(\boldsymbol{mK/W})$	$\boldsymbol{q'_{input}}$ $(\boldsymbol{W/m})$	$\boldsymbol{q_{input}}$ $(\boldsymbol{kW})$
5.5	412.12	0.65	1.29
6	381.75	0.69	1.40
7	332.76	0.80	1.60
10	240.36	1.11	2.22
14	175.48	1.52	3.04

Comparing the heat inputs obtained per unit length, q'_{input}, with values found in literature, it is concluded that the results of Table 4.4 are optimistic. For example, Mangold (2022) considers an incoming heat flow of 3.5 W/m occurring in a 12-inch distribution pipeline. This heat flow rate is over twice the input obtained in Table 4.4 for the largest duct studied, 14-inch diameter. This is a considerable difference, and it can be because heat transfer through structural supports, pipe segment connections and relief valves is not taken into account in this analysis. To remedy this issue, the missing heat input is considered by Verstraete (2009) as an additional 30% margin, i.e., multiplying the heat penetration by a 1.3 correction factor. Researchers have not yet reached a consensus on quantifying this additional heat input as it also depends on how the supports are designed. However, comparing the results obtained with the literature, it may seem that a correction factor higher than 1.3 should be used. Different insulation correction factors, from better to worse thermal performance, are applied and discussed below.

So far, it has been observed that the larger the pipe diameter, the lower the flow speed and the greater the heat input from the outside per unit hydrogen into the pipe core and, consequently, the boil-off. However, it cannot be concluded that the 5.5-inch pipe is the most suitable size to minimize BO as the heat added by the pumping group and heat added by friction must still be analyzed.

4.1.1.2. Analysis of the heat added by the pumping group and by friction

The heat contributions of the pumping group and friction for the previous five diameters are addressed. The strategies described in sections 3.2.2.2 and 3.2.2.3 are followed to quantify each heat contribution.

First, the heat produced by the pump is studied. The pumping group is responsible for providing the flow with the mechanical energy required to overcome friction along the whole pipeline and delivering LH_2 at the correct pressure at the stand transfer tank. Therefore, the pumping group must be sized to meet the airport demand requirements and operating conditions.

The first step to sizing the pump is to obtain the suction and discharge pressure, calculated from the storage farm pressure, 1.1 bar, the minimum supply pressure at the stand, 1.5 bar, and the pressure losses along the facility due to friction. Endpoint

pressures are fixed so that the results will depend directly on the different friction effects, which depend on the fluid speed and the size and length of the pipe. To simplify the reading of the results, primary and secondary pressure losses are shown together, and the facility is divided into two segments: segment one upstream of the pumping group and segment two immediately downstream. Pressure losses are denoted as h_i, where i refers to the corresponding segment. All pressures are measured in meters of liquid hydrogen column. Thus, the storage farm and supply pressures are equal to $p_{storage} = 157.93m$ and $p_{supply} = 215.36m$.

Table 4.5: Operating pressures of the pumping group and pressure losses along the facility per different pipe sizes.

$\boldsymbol{Pipe\ size}$ $(\boldsymbol{in})$	$\boldsymbol{h_1}$ $(\boldsymbol{m})$	$\boldsymbol{p_{suction}}$ $(\boldsymbol{m})$	$\boldsymbol{p_{discharge}}$ $(\boldsymbol{m})$	$\boldsymbol{h_2}$ $(\boldsymbol{m})$
5.5	0.61	157.32	1029.65	813.91
6	0.379	157.55	720.77	505.41
7	0.164	157.77	433.89	218.53
10	0.024	157.91	247.54	32.18
14	4.07E-03	157.93	220.79	5.43

From Table 4.5, it can be observed that pressure losses between the storage tank and the pump are comparatively minimal, as the pipe segment is short. Therefore, h_1 can be neglected. In the case of the second pipe segment, the pressure losses, h_2, increase considerably the smaller the pipe size. This supposes that the pumping group must provide a higher pressure to the fluid to overcome the frictional forces within the duct, and, consequently, the pump power requirements must be higher.

Using the previous suction and discharge pressures the pump head, H_p, required for each diameter is obtained. Then, according to Equation (3.15), the required power of the pumping group is calculated. Last, the total heat added to the LH_2 flow is estimated from the pump efficiency, $\eta = 0.73$ (Mangold et al. 2022).

Table 4.6: Pump head, H_p, pump power, P_{pump}, and total heat added to the LH_2 flow by the pumping group, q_{pump}, for each pipe size.

$\boldsymbol{Pipe\ size}$ $(\boldsymbol{in})$	$\boldsymbol{H_p}$ $(\boldsymbol{m})$	$\boldsymbol{P_{pump}}$ $(\boldsymbol{kW})$	$\boldsymbol{q_{pump}}$ $(\boldsymbol{kW})$
5.5	871.95	87.58	23.65
6	563.22	56.57	15.27
7	276.12	27.73	7.49
10	89.63	9.00	2.43
14	62.86	6.31	1.70

Therefore, Table 4.6 shows that working with a constant mass flow of 7.47 kg/s, the heat added by the pumping group to the fluid increases considerably at high flow speeds as the pipe size becomes smaller and frictional forces gain importance. Consequently, there will be a large difference between the BO occurring along the smallest pipeline and the largest one. However, while it is true that choosing the largest pipe size would minimize the BO, it may mean oversizing the installation unnecessarily. The high construction cost could reduce the potential savings from lower BO.

To check the reliability of the power requirements obtained in Table 4.6, they are again compared with the literature. In their work, Mangold et al. (2022) describe a distribution system consisting of a 12-inch pipe and a mass flow rate of 40 kg/s. That airport has no stand transfer tanks so the fluid must be supplied to the hydrant at 7 bar pressure. Considering a pump efficiency of 0.73, the power of the pumping group required under those conditions is 660 kW. The same operating conditions have been introduced into the model of this thesis and a pumping power of 640.3 kW has been obtained. This shows, therefore, that the results obtained in Table 4.6 are of comparable magnitude and that other authors have used similar calculation procedures.

Following a similar reasoning, described in section 3.2.2.3, the heat added to the flow by friction between the fluid and the duct walls is analyzed. Considering the mass flow and the sum of the pressure losses in both segments of the distribution pipe, the heat added by friction is obtained through Equation (3.18). Pressure losses are shown above in Table 4.5.

Table 4.7: Total heat added to the LH_2 flow by friction, $q_{friction}$, for the different pipe diameters.

$\boldsymbol{Pipe\ size}$ $(\boldsymbol{in})$	$\boldsymbol{q_{friction}}$ $(\boldsymbol{kW})$
5.5	59.72
6	37.08
7	16.03
10	2.36
14	0.39

The results in Table 4.7 are in line with those obtained in Table 4.6 for the heat added by the pump. At equal mass flow, the effect of friction is much more dominant within small pipes and therefore the thermal energy provided to the fluid is much higher.

4.1.1.3. Analysis of the total heat added to the LH_2 flow and boil-offs

The analysis of the total heat added to the fluid along the defined distribution scenario for different pipe diameters is summarized in the following table.

Table 4.8: Summary of the different heat source contributions and total heat added to the fluid, q_{total}, along the distribution pipeline.

$\boldsymbol{Pipe\ size}$ $(\boldsymbol{in})$	$\boldsymbol{q_{input}}$ $(\boldsymbol{kW})$	$\boldsymbol{q_{pump}}$ $(\boldsymbol{kW})$	$\boldsymbol{q_{friction}}$ $(\boldsymbol{kW})$	$\boldsymbol{q_{total}}$ $(\boldsymbol{kW})$
5.5	1.29	23.65	59.72	84.66
6	1.40	15.27	37.08	53.75
7	1.60	7.49	16.03	25.12
10	2.22	2.43	2.36	7.01
14	3.04	1.70	0.39	5.14

From the data in Table 4.8 and the latent heat of vaporization, ΔH_{vap}^{LH2}, the boil-offs are calculated for each diameter.

Table 4.9: Summary of boil-offs occurring in the distribution pipeline for different diameters at the base case.

$\boldsymbol{Pipe\ size}$ $(\boldsymbol{in})$	$\boldsymbol{\dot{m}_{input\ BOL}}$ $(\boldsymbol{g/s})$	$\boldsymbol{\dot{m}_{pump\ BOL}}$ $(\boldsymbol{g/s})$	$\boldsymbol{\dot{m}_{friction\ BOL}}$ $(\boldsymbol{g/s})$	$\boldsymbol{\dot{m}_{total\ BOL}}$ $(\boldsymbol{g/s})$
5.5	2.89	52.89	133.60	189.39
6	3.12	34.17	82.96	120.26
7	3.58	16.75	35.87	56.21
10	4.96	5.44	5.28	15.68
14	6.80	3.81	0.89	11.50

The data in Table 4.9 has been plotted to visually compare the importance of each contribution to the total boil-off for each diameter.

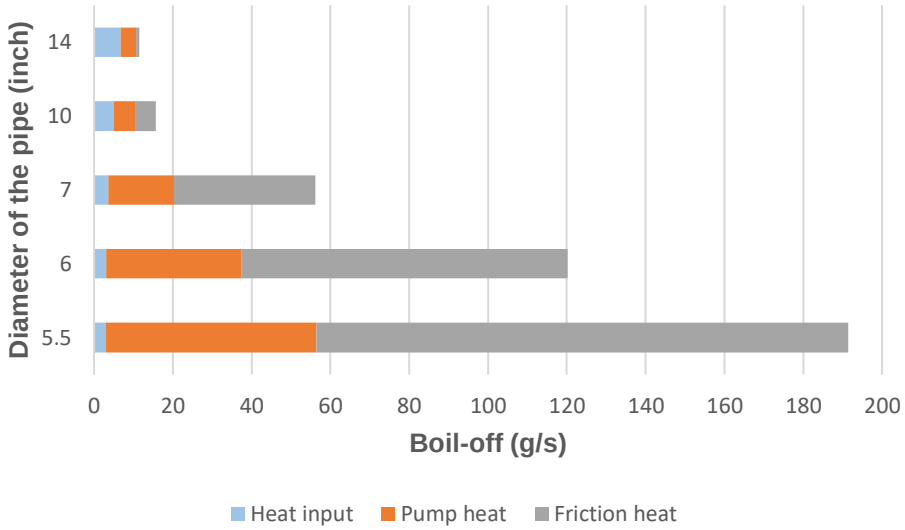

Figure 4.1: Comparison of the contributions to boil-offs for the different pipe diameters in the base case.

Figure 4.1 shows that the total BO increase considerably for smaller diameters. Indeed, the boil-offs for the 14-inch diameter are roughly 94% lower than for the 5.5-inch diameter. Furthermore, it can be seen that the heat transfer from the outside behaves oppositely to the other two heat sources: the pump and the friction. BO due to heat input are comparatively minimal in small pipes. However, they gain importance as the diameter of the pipe increases, becoming the major boil-offs for the 14-inch diameter. The opposite is true for pump and friction BO. They present high values with smaller diameter pipes and decrease notably as the pipe increases. The decrease is especially remarkable for friction BO, which become the smallest contribution in the 14-inch diameter.

These tendencies are shown in the following figure, where the relative distribution of BO in each case is plotted. It is observed that pump BO, although decreasing, remain at around 30% of total BO in all cases.

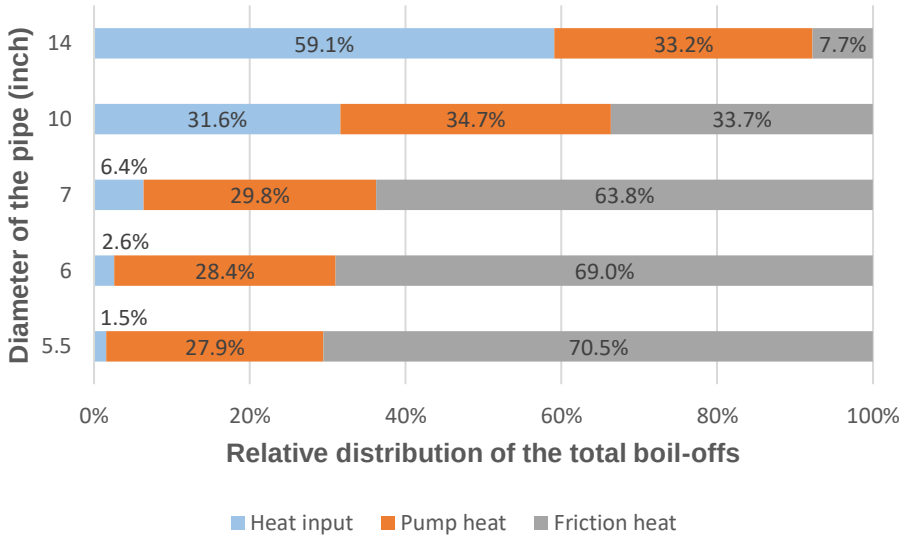

Figure 4.2: Distribution of BO per group for the different diameters in the base case.

Furthermore, the obtained results are in line with Brewer's suggested minimum pipe diameter. The author claims that the distribution pipe should be larger than 10 inches (254 mm) to reduce friction within the duct. Indeed, at the 10-inch diameter, the contribution of the three groups to the total BO is almost identical. From this size onwards, according to the trend, boil-off due to heat input become the dominant group. At this point it can be stated that the most suitable diameter for the distribution facility applying the assumptions described will be between 10 and 14 inches.

To better understand the magnitude and relevance of the results in Table 4.9, the boil-off rates are calculated with respect to the delivered mass flow. In addition, the total tons of BO at the end of the day, m_{BOL}^{total}, are shown. These values help to realize the considerable impact that BO can have on the airport's operation and economy.

Table 4.10: Boil-off rates compared to the LH_2 flow and daily tons of boil-off gases along the pipeline distribution system.

$\boldsymbol{Pipe\ size}$ $\boldsymbol{(in)}$	$\boldsymbol{Boil-off\ rate}$ (%)	$\boldsymbol{m_{BOL}^{total}}$ $\boldsymbol{(t\ GH2/day)}$
5.5	2.56	16.54
6	1.61	10.39
7	0.75	4.86
10	0.21	1.35
14	0.15	1

It should be noted that the results in Table 4.10 represent only the BO occurring within the pipeline. Additional losses are expected at the storage facility, upon transfer and

upon refueling. The results reflect the importance of minimizing boil-off and the need to build a recovery infrastructure at the airport. Otherwise, boil-off losses would lead to a considerable economic impact on airport operating costs and a large volume of hydrogen emissions into the atmosphere, impacting the environment. The future goal is to achieve distribution systems with virtually zero boil-off or at least procuring a high recovery rate at the airport. This is vital because with the lowest boil-off rate obtained in the table above, i.e., 1,000 kg H_2, a Caetano fuel cell city bus could travel 16,600 km (CaetanoBus, 2019). This distance is a quarter of the average annual mileage of a city bus. Therefore, an extensive BO infrastructure will be needed at the airport. This will also make it possible to decarbonize many of the airport's services and even turn the airport into a hydrogen hub.

Comparing these results with the literature, Brewer (1976) states in his work that the boil-offs in a 8-inch (203 mm) pipe delivering 7.68 kg/s from a liquefaction plant to the airport represent 0.3% of the total mass flow over a 1,600 m pipe. This boil-off rate is relatively similar to that obtained for the 10-inch pipe in Table 4.10 and therefore demonstrates that the results are in line with the literature.

4.1.2. Choice of pipe diameter

In the previous subsection a comprehensive study of the influence of pipe diameter on the BO has been made. With these results, it is very likely that the most appropriate diameter for the distribution base case is between 10 and 14 inches. However, to make the final decision it should be checked that the above diameters respect the flow speed limits, Equation (4.1) and (4.2), in different LH_2 demand situations, both lower and greater.

First, a lower consumption scenario is analyzed. Before setting the new LH_2 demand, recalling Table 4.1, it is possible to discard the 14-inch diameter because if the mass flow decreases the flow velocity will fall below the limit, 1 m/s. Based on the 2019 Munich airport traffic report, February is the month with the lowest aircraft movements, which dropped 21% compared to September (Munich Airport, 2019b). Daily LH_2 consumption is assumed to follow the same trend, so that the minimum demand is set at 79% of the September fuel requirement, i.e., 510 tons LH_2 per day. Again, the mass flow is considered constant throughout the day and its value is set at 5.9 kg/s. Under this new scenario, a 13-inch pipe is the one that provides the lowest boil-off rate while respecting the minimum fluid speed. This pipe size will also be appropriate for the intermediate consumptions between February and August values.

On the other hand, possible scenarios with higher demand for LH_2 should be analyzed. In favor of the defined distribution system is the existence of transfer tanks at the stands, which makes it possible to decouple distribution from refueling partially. As the transfer tanks can be constantly refilled, several aircraft can be refueled simultaneously from their respective intermediate tanks without affecting the mass flow of the backbone pipeline. This is the drawback of the systems described by Brewer (1976) and Mangold et al. (2022). Those layouts do not have stand tanks, thus, high mass flows in the main pipeline are required to be able to refuel two aircraft simultaneously at an energy flow rate of 2100 MJ/s per plane, i.e., 17.5 kg/s of LH_2. This energy rate is the current value used for kerosene and must be maintained in order not to increase turnaround times (Mangold et al., 2022). Therefore, with the chosen distribution configuration, it is unlikely that such large flows will be required. However, if necessary, the 13-inch pipe could deliver up to

42.37 kg/s according to the speed constraint (4.3). For all these reasons, it is decided to set the pipe diameter at 13 inches as the most appropriate for the base case.

In the event of a drastic and prolonged drop in LH_2 consumption that make impossible to comply the minimum flow speed, for some exceptional reason, such as a new pandemic, refueling trucks could be used instead or even a smaller redundant distribution pipeline. Both options would also be suitable to solve the opposite situation, i.e., to support the backbone pipeline during an episode of exceptionally high demand.

4.2. Study of the 13-inch pipeline distribution system

Once the diameter of the distribution pipe has been selected, the basic pipe characteristics are calculated and the performance of the distribution system under different conditions is studied.

4.2.1. Characterization of the pipeline

Before analyzing the boil-offs occurring in the distribution system, the basic characteristics of the 13-inch diameter pipe are presented. The pipe structure and materials used remain the same. The thermal properties and thicknesses of each layer are taken from Table 3.1. From these values the exact sizes of each layer of the 13-inch pipe and their linear thermal resistances are defined.

Table 4.11: Physical characteristics of the 13-inch distribution pipeline.

$\boldsymbol{Layers}$	$\boldsymbol{Outer\ diameters}$ $(\boldsymbol{mm})$	$\boldsymbol{R_i'}$ $(\boldsymbol{mK/W})$
Inner pipe	330.2 (13 inch)	2.07E-04
Insulation	333.84	12.92
Evacuated annulus	372.7	175.25
Outer pipe	381.08	2.18E-04

The equivalent linear thermal resistance of the pipe, $\boldsymbol{R'_{equiv}}$, takes a value of $188.17 mK/W$. As explained above, this information is essential to quantify the total amount of heat provided to the LH_2 flow and, consequently, the BO. Regarding the heat input from the outside, in this study it is decided to use as a reference a correction factor of 2 to account for heat entering through poorly insulated elements such as structural supports, pipe joints and relief valves. The recommendation to use a correction factor was already introduced in section 4.1.1.1.

4.2.2. Average boil-offs at the base case airport

Once the characteristics of the chosen pipe have been defined, the boil-off occurring in the distribution system are studied. To this end, average operating conditions at the airport must be set. Therefore, it is decided to calculate reference conditions based on public information on the monthly consumption and temperature evolution at Munich airport throughout the year. From the monthly aircraft movements (Munich Airport,

2019b) and considering that the busiest month, September, requires 615 tons/day of fuel, the LH_2 demand for the remaining months can be defined. The proposed consumptions and constant mass flows, and the monthly average temperatures during the year in Munich are shown in Table 4.12.

Table 4.12: Expected variations in LH_2 consumption and temperature over the year in Munich area (Munich Airport, 2019b; Weather Spark, 2023).

$\boldsymbol{Month}$	$\boldsymbol{Consumption}$ $(\boldsymbol{ton/day})$	$\dot{\boldsymbol{m}}$ $(\boldsymbol{kg/s})$	$\boldsymbol{T_{amb}}$ (℃)
January	508	6.17	-1
February	48	5.91	0
March	557	6.77	4
April	554	6.73	8
May	609	7.40	13
June	592	7.19	16
July	612	7.44	18
August	587	7.13	18
September	615	7.47	14
October	606	7.36	9
November	511	6.21	4
December	509	6.18	1

To facilitate the analysis of above data, they are plotted in a graph. Figure 4.3 shows the percentage variation of monthly consumption with respect to the maximum demand,

occurring in September. At the same time, the fluctuation of the average temperature is also plotted.

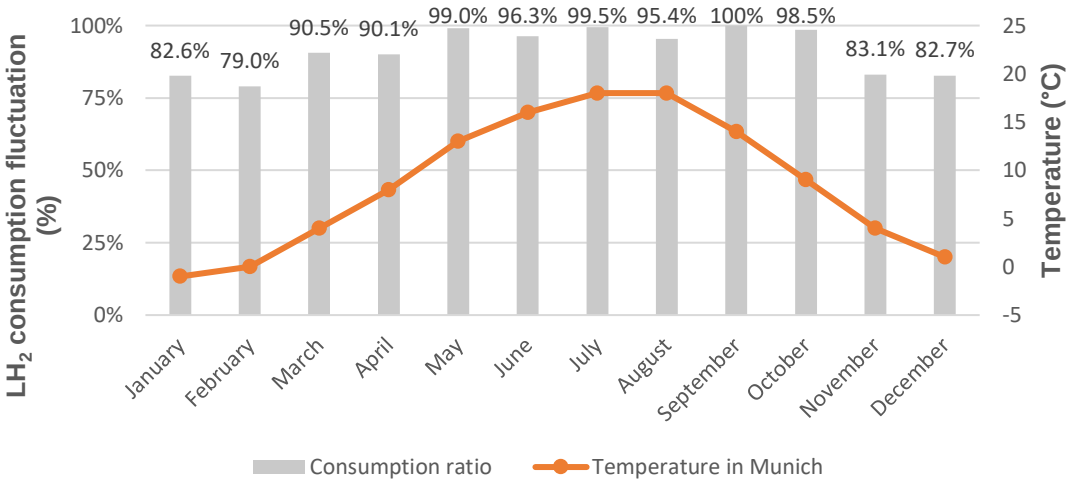

Figure 4.3: Representation of the monthly consumption fluctuations compared to peak value and temperature during the year in Munich (Table 4.12).

The above graph shows that the highest consumptions are grouped between March and October, which coincide with the warmest seasons in Munich. From November to February, temperatures plummet to around 0°C and monthly consumption drops by about 20% compared to peak consumption. Having pointed out this trend, the average scenario over the year is defined.

Table 4.13: Average consumption and temperature in Munich.

Conditions	***Average values***	***Units***
LH_2 daily consumption	562	(ton/day)
Mass flow, $\dot{m}$	6.83	(kg/s)
Temperature, T_{amb}	8.67	$(°C)$

The other elements necessary to calculate the boil-offs remain the same as described in Table 3.2. Therefore, the operating conditions and BO results obtained for the 13-inch diameter distribution system are shown in Table 4.14.

Table 4.14: Average conditions consumption and temperature values throughout the year in Munich.

Conditions	***Average values***	***Units***
Daily LH_2 consumption	562	(ton/day)
Mass flow, $\dot{m}$	6.83	(kg/s)
Temperature, T_{amb}	8.67	$(°C)$
Correction factor	2	–
Flow speed, v	1.17	(m/s)
Reynolds, Re	2.07E+06	–
Friction factor, f	0.0148	–
Pumping requirements	***Average values***	***Units***
Discharge pressure, $p_{discharge}$	222.07	(m)
Pump head, H_p	64.15	(m)
Pump power, P_{pump}	5.9	(kW)
Motor power, P_{el}	7.21	(kW)
Boil − offs	***Average values***	***Units***
Heat input BO, $\dot{m}_{input\ BO}$	12.42	(g/s)
Pump BO, $\dot{m}_{pump\ BO}$	3.56	(g/s)
Friction BO, $\dot{m}_{friction\ BO}$	1.01	(g/s)
Daily heat input BO	1,073.1	(kg/day)
Daily pump BO	307.5	(kg/day)
Daily friction BO	87.2	(kg/day)
Total BO, $\dot{m}_{total\ BO}$	17	(g/s)
Daily total boilf-offs	1,467.8	(kg/day)
Boil-off rate	0.25	$(\%)$

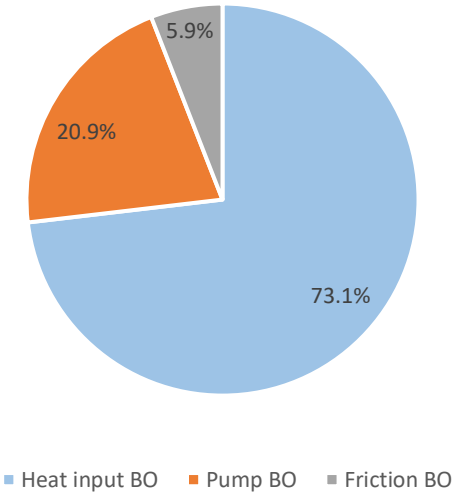

Figure 4.4: Average contribution of each heat source to the total boil-offs along the 13-inch distribution pipeline.

From the electrical power of the pumping group, 7.21 kW, the average daily consumption of the distribution system can be calculated. Considering that the installation operates all day long, the energy consumed is 173 kWh. This energy could be obtained from a fuel cell system by transforming the boil-off gases recovered into electricity. According to the energy density of hydrogen, 5.2 kg of LH_2 would be sufficient to power the distribution system, which is negligible compared to the total BO. The total boil-off per day, 1,467.8 kg, represents an enormous amount of energy that could power 3.3 regional flights with a mission range of 750 km (Lopez, 2022; Mukhopadhaya & Rutherford, 2022). In terms of energy, the daily boil-off is equivalent to 48.9 MWh. Annual electricity consumption at Munich Airport in 2018 was 232,675 MWh, i.e., approximately 637.5 MWh per day (Munich Airport, 2019a). Therefore, around 8% of the airport's electricity demand could be met by recovering BO gases and transforming them into electricity.

Ultimately, a large infrastructure for recovery, storage and utilization of boil-off gases will be needed at airports using LH_2. Although the recovered hydrogen can be used for a multitude of applications, it is highly desirable to minimize boil-offs. A very large boil-off volume would result in higher energy consumption associated with H_2 treatment, increased demand for airport space, and increased risks associated with cryogenic fluid handling. In any case, efficient handling and use of boil-off gases will be crucial for hydrogen-based aviation to be economically viable.

4.3. Parametric analyses

A parametric analysis is carried out in which certain parameters are modified with respect to the base case of 13 inches of pipe. The parameters analyzed are the insulation correction factor, ambient temperature, pipe length, pumping group performance, supply pressure and mass flow. The objectives of these parametric analyses are several:

- Checking the robustness of the model and analyzing whether congruent results are obtained beyond the average scenario. It allows the detection of possible errors.

- Identifying the most influential input variables in the model and quantifying their impact on the results. In addition, the relationship between the intervening variables is studied in more detail.

- To provide further understanding of the BO occurring in LH_2 pipeline distribution. This will support designers and decision-makers with more information when developing such a project.

Only one factor is studied per analysis, one-factor-at-a-time, to better understand each individual contribution to the model results.

4.3.1. Insulation correction factor (ICF)

As discussed in section 4.1.1.1, due to missing experience with large scale LH2 pipeline distribution it is unclear how much heat transfer may occur through insufficiently insulated elements along the pipe. In the average case, an insulation correction factor (ICF) of 2 is considered. To study the impact this decision may have on the model results, the study is carried out for coefficients ranging from 50% to 160% with respect to the average ICF.

Figure 4.5 shows the resulting boil-offs per day for each case. A linear increase in the total boil-offs is observed as the ICF increases. The contributions of the pumping group and friction remain constant, and only the heat input BO increase.

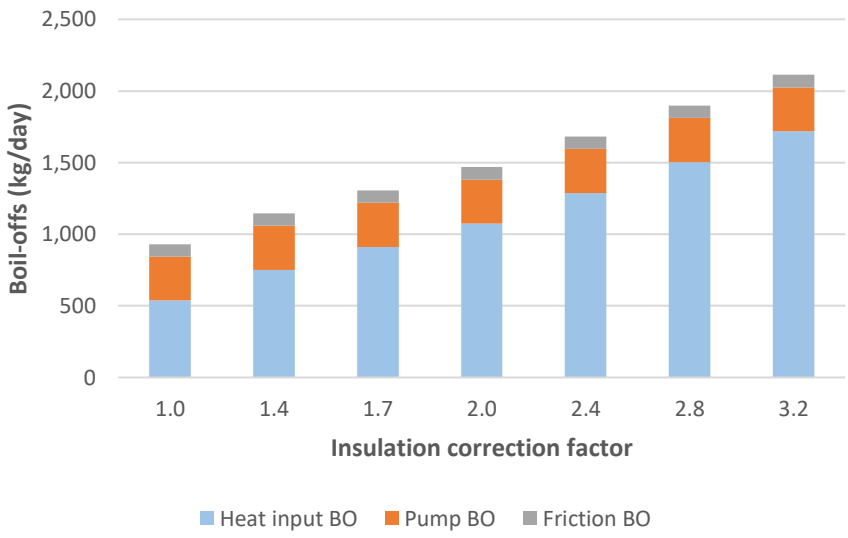

Figure 4.5: Comparison of daily boil-offs as a function of the assumed insulation correction factor.

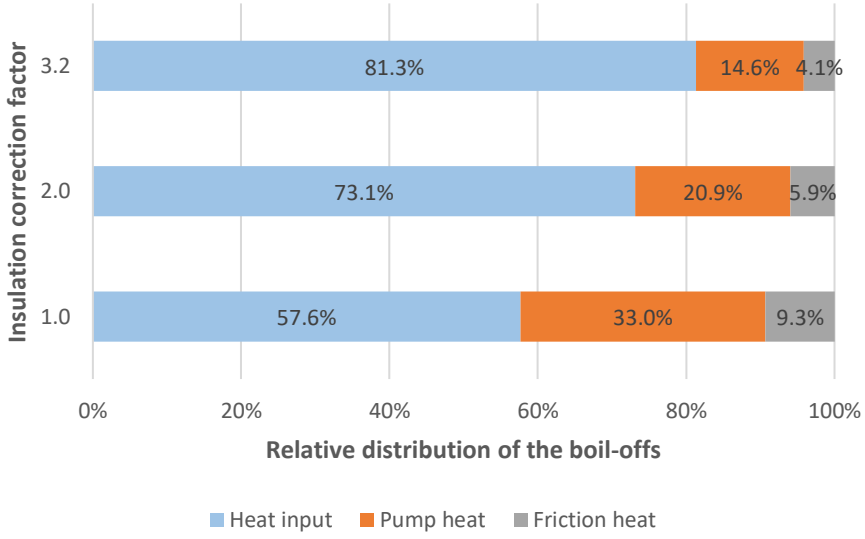

Figure 4.6: Distribution of boil-offs per heat source for the different insulation correction factors.

Figure 4.7 shows the boil-off rates obtained for each ICF analyzed. These values are calculated by dividing the total BO by the daily consumption of the average case. The boil-off rate is a good indicator to describe the performance of the distribution system and it is important to keep it as low as possible.

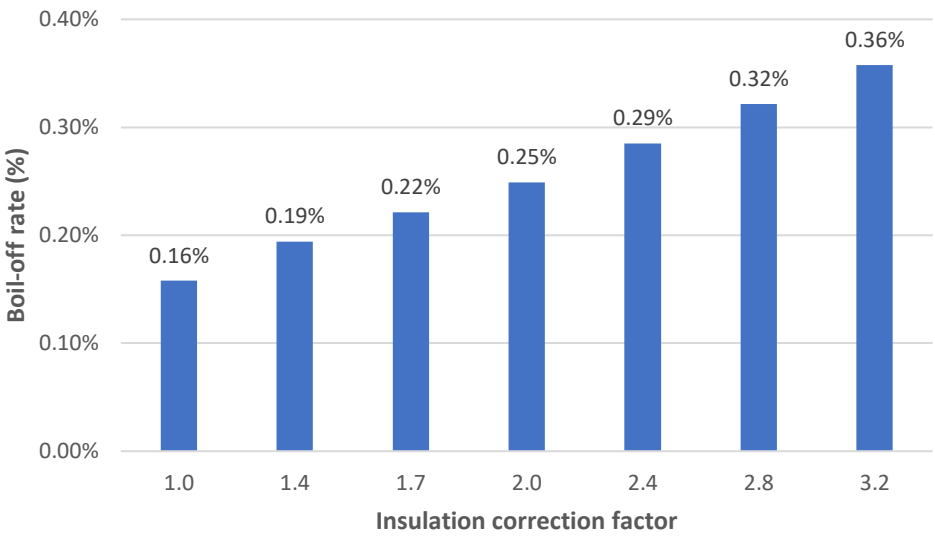

Figure 4.7: Resulting boil-off rates in the distribution system for each of the insulation correction factors analyzed.

The following tables show the results obtained for each ICF. In addition, the results are compared with respect to the average case and each variation is shown as a percentage. Table 4.15 shows only the variations on heat input boil-offs, while Table 4.16 shows the impact of the assumed ICF on the total boil-offs.

Table 4.15: Comparison of heat input BO depending on the assumed ICF and percentage variation with respect to the average case.

ICF	$ICF\ fraction$	$Heat\ input\ BO\ (kg/day)$	$Input\ BO\ variation\ from\ average\ case\ (\%)$
1	0.5	536.74	-50
1.4	0.7	751.44	-30
1.7	0.85	912.46	-15
2	1	1,073.49	–
2.4	1.2	1,288.18	20
2.8	1.4	1,502.88	40
3.2	1.6	1,717.58	60

Table 4.16: Comparison of total BO depending on the assumed ICF and percentage variation with respect to the average case.

ICF	$ICF\ fraction$	$Total\ BO\ (kg/day)$	$Total\ BO\ variation\ from\ average\ case\ (\%)$
1	0.5	931	-36.6
1.4	0.7	1,146	-21.9
1.7	0.85	1,307	-11.0
2	1	1,468	–
2.4	1.2	1,683	14.6
2.8	1.4	1,897	29.3
3.2	1.6	2,112	43.9

In view of these results, it can be seen that the choice of the ICF has a significant influence on the calculation of boil-offs. The assumed ICF directly impacts the heat input BO and the results are proportional to the value chosen. To avoid large deviations between calculations and actual boil-offs in the distribution system it will be crucial to assume the most accurate ICF possible when designing the airport. Failure to do so may result in an incorrect sizing of the boil-off recovery infrastructure. Furthermore, this showcases the critical importance of an optimized design of the supports, valves and other in-pipe components.

4.3.2. Ambient temperature

In section 4.2.2 the average annual temperature of Munich, roughly 9ºC, was calculated. From this ambient temperature and the average consumption, the BO were obtained. This section studies to what extent the outside temperature affects the BO when all other parameters remain unchanged. Therefore, six different temperatures are established and compared with respect to the average temperature in Munich. The temperatures are: -7, 0, 5, 9, 15, 24 and 36°C. These values can be considered as seasonal temperature fluctuations in Munich or as the average temperature in other geographical locations.

The figure below shows the BO obtained for each ambient temperature. A slight increase in boil-offs is observed as the temperature increases. The opposite occurs if the temperature drops. Lower temperatures slightly reduce boil-offs. As in the ICF analysis, only the BO originated from the heat input vary, while the other two groups remain constant.

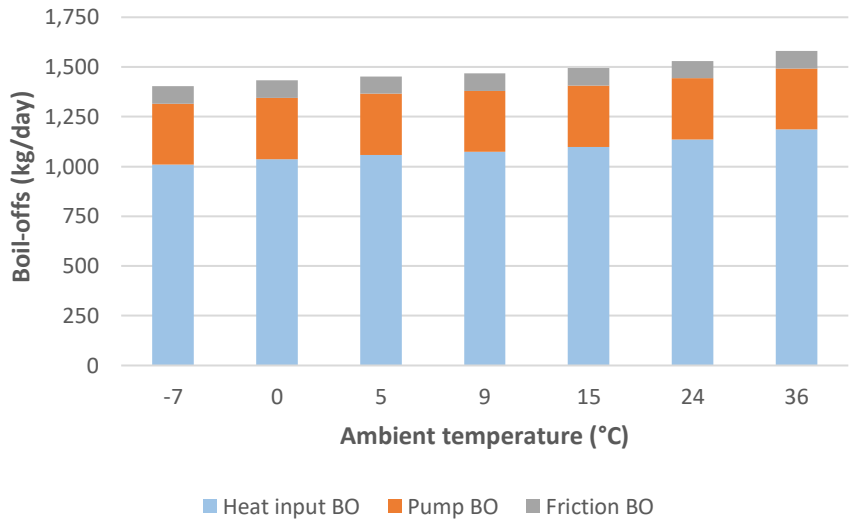

Figure 4.8: Comparison of daily boil-offs as a function of the ambient temperature.

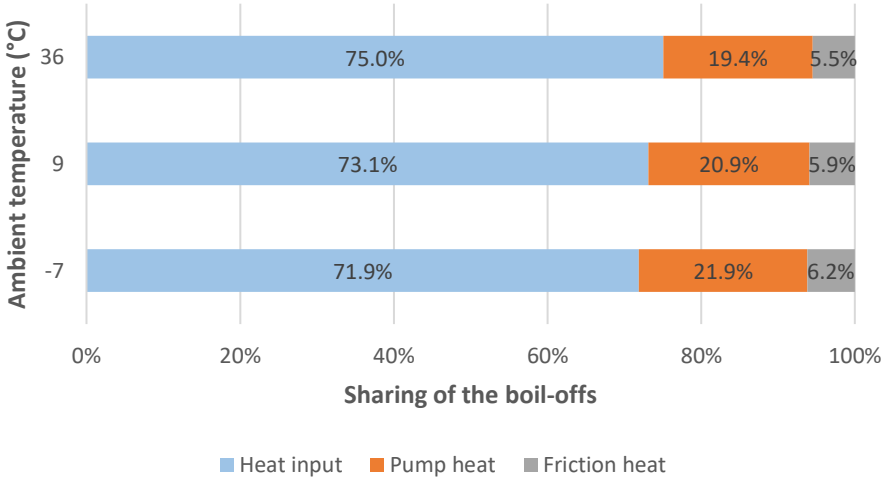

Figure 4.9: Distribution of boil-offs per heat source for the different ambient temperatures.

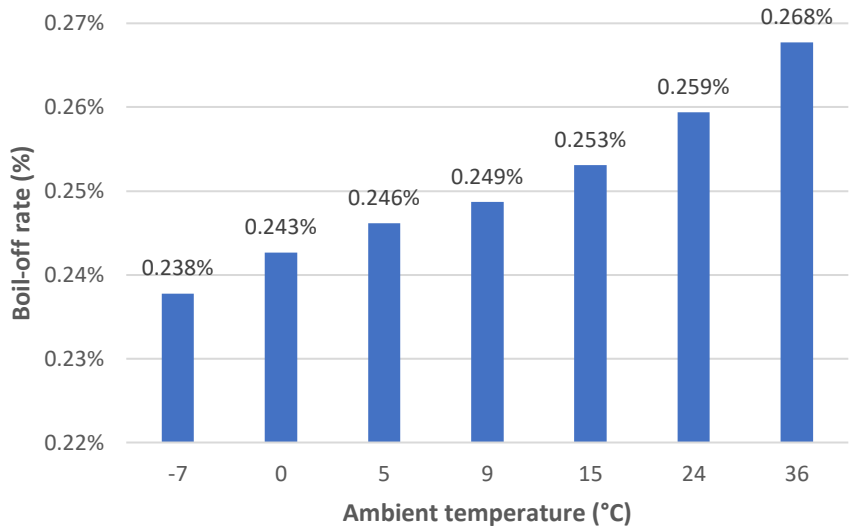

Figure 4.10: Resulting boil-off rates in the distribution system for each of the ambient temperatures analyzed.

The results of the analysis are shown in the following tables. The results are compared with respect to the average case and each variation in BO resulting from the temperature difference is shown as a percentage. Table 4.17 refers only to changes in heat input BO while Table 4.18 shows the percentage variation in total boil-offs.

Table 4.17: Comparison of heat input BO depending on the ambient temperature and percentage variation with respect to the average case.

$\boldsymbol{Ambient\ temperature}$ (℃)	$\boldsymbol{Temperature\ difference}$ (℃)	$\boldsymbol{Input\ BO}$ $(\boldsymbol{kg/day})$	$\boldsymbol{Input\ BO\ variation\ from\ average\ case}$ (%)
-7	-16	1,009	-6.00
0	-9	1,038	-3.32
5	-4	1,058	-1.40
9	0	1,073	–
15	6	1,099	2.42
24	15	1,136	5.87
36	27	1,186	10.46

Table 4.18: Comparison of total BO depending on the ambient temperature and percentage variation with respect to the average case.

$\boldsymbol{Ambient\ temperature}$ (℃)	$\boldsymbol{Temperature\ difference}$ (℃)	$\boldsymbol{Total\ BO}$ $(\boldsymbol{kg/day})$	$\boldsymbol{Total\ BO\ variation\ from\ average\ case}$ (%)
-7	-16	1,403	-4.39
0	-9	1,432	-2.43
5	-4	1,453	-1.03
9	0	1,468	–
15	6	1,494	1.77
24	15	1,531	4.29
36	27	1,580	7.65

The results show that the ambient temperature does not play a determining role in the behavior of the model. This is due to the extremely low boiling point of the LH_2. In fact, a temperature difference of 15°C only represents an increase of around 4% of the total boil-offs. In addition, an average temperature above 36ºC, which is unlikely to occur over long periods of time, is also analyzed. This temperature shows that even such high temperatures do not significantly impact the total BO. Therefore, it can be concluded that the maximum impact on the BO due to ambient temperature change will not exceed a difference of 10% with respect to the average case considering earth's ambient.

4.3.3. Length of the distribution pipe

The length of the distribution pipe is a key parameter within the model and should be reduced to the minimum necessary to avoid exposure of the cryogenic fluid. In the base case an average length of 2,000 m is considered. It is imposed that the pipe must measure less than 3,500 m, therefore the influence of the pipe length is analyzed within the range of 60% to 160% of the length of the base case.

Figure 4.11 shows the BO obtained for the different pipe lengths analyzed. As expected, the increase in pipe length is accompanied by a significant increase in the total BO. At first glance, the increase is noticeably higher within the heat input group, as the pipe surface increases proportionally with the length. The pump and friction BO also increase as the pipeline grows, although in a softer way. This makes sense since the pipe length is directly related to the friction pressure losses through the *Darcy-Weisbach* formula, Equation (3.6).

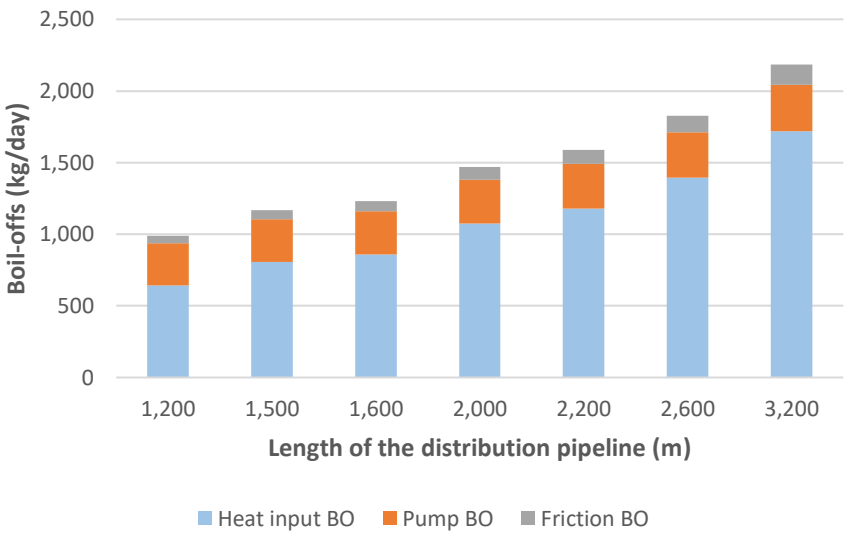

Figure 4.11: Comparison of daily boil-offs as a function of the length of the distribution pipeline.

The contribution of each group to the total boil-offs is shown in Figure 4.12. Not all lengths are plotted in the figure because the trend is well defined with the extreme cases and the average case.

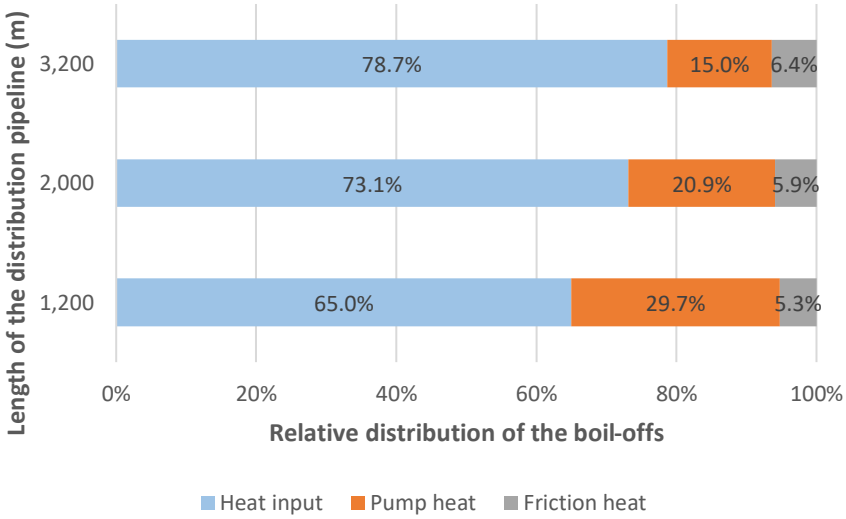

Figure 4.12: Distribution of boil-offs per heat source for the different pipeline lengths.

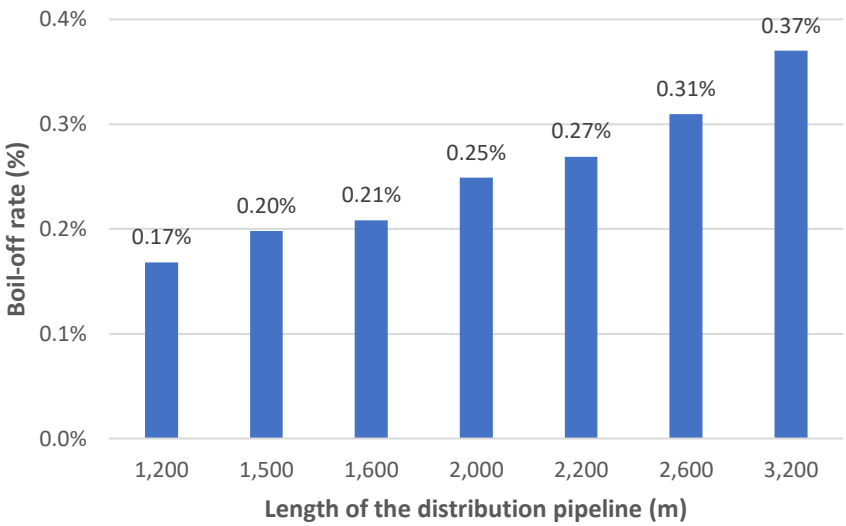

Figure 4.13: Resulting boil-off rates in the distribution system for each of the pipe lengths analyzed.

The resulting boil-offs from each heat category as a function of the pipe length and the variations with respect to the average case are shown in the following tables. Both the heat input and friction BO show variations equal to the fraction between pipe lengths. Therefore, the friction BO table is omitted below.

Table 4.19: Comparison of heat input BO depending on the pipe length and percentage variation with respect to the average case.

$\boldsymbol{Pipe\ length\ (m)}$	$\boldsymbol{Pipe\ length\ fraction}$	$\boldsymbol{Heat\ input\ BO\ (kg/day)}$	$\boldsymbol{Input\ BO\ variation\ from\ average\ case\ (\%)}$
1,200	0.6	644	-40
1,500	0.75	805	-25
1,600	0.8	859	-20
2,000	1	1,073	–
2,200	1.1	1,181	10
2,600	1.3	1,396	30
3,200	1.6	1,718	60

In the ICF and temperature analyses the characteristics of the pumping group remain the same. In this case, however, if the length of the pipeline is modified, the requirements of the pumping group change. The increase in the pipe length implies an increase in pressure losses due to friction, and consequently the power required from the pumping group to overcome friction is greater. The increase in pump work means a slight increase in the heat added to the fluid and therefore in the BO. As shown in Table 4.20, the lengths

analyzed produce increments of less than 10% in the pump BO and power of the pumping group with respect to the average case.

Table 4.20: Comparison of pump BO and pump power depending on the pipe length and percentage variation with respect to the average case.

$\boldsymbol{Pipe\ length}$ $(\boldsymbol{m})$	$\boldsymbol{Pipe\ length\ fraction}$	$\boldsymbol{Pump\ BO}$ $(\boldsymbol{kg/day})$	$\boldsymbol{Pump\ power}$ $(\boldsymbol{kW})$	$\boldsymbol{Variation\ from\ average\ case}$ (%)
1,200	0.6	294	5.64	-4.19
1,500	0.75	299	5.73	-2.62
1,600	0.8	301	5.77	-2.09
2,000	1	307	5.89	–
2,200	1.1	311	5.95	1.05
2,600	1.3	317	6.07	3.14
3,200	1.6	327	6.26	6.28

Table 4.21: Comparison of total BO depending on the pipe length and percentage variation with respect to the average case.

$\boldsymbol{Pipe\ length}$ $(\boldsymbol{m})$	$\boldsymbol{Pipe\ length\ fraction}$	$\boldsymbol{Total\ BO}$ $(\boldsymbol{kg/day})$	$\boldsymbol{Total\ BO\ variation\ from\ average\ case}$ (%)
1,200	0.6	991	-32.5
1,500	0.75	1,170	-20.3
1,600	0.8	1,229	-16.2
2,000	1	1,468	–
2,200	1.1	1,587	8.1
2,600	1.3	1,826	24.4
3,200	1.6	2,183	48.7

Table 4.21 shows the impact of changing the pipe length on total BO with respect to the average case. The results confirm that length is a critical factor in the piping distribution system and should be given careful consideration during airport layout design. The longer the length of the pipeline distribution system, the higher the boil-off rate.

4.3.4. Mass flow

In this case, the impact of the mass flow on BO along the distribution system is analyzed. For this purpose, a series of different mass flow rates ranging from 87% to 256% of the average case are defined. The first two mass flows studied, 5.9 and 7.5 kg/s, correspond to the months with the lowest and highest demand in the average case. The minimum mass flow studied must respect the fluid speed limitations, $v > 1 m/s$, therefore the analysis cannot be performed with flow rates lower than 5.9 kg/s. The highest flow rate studied is 17.5 kg/s, which according to Mangold et al. (2022) is the flow rate necessary to refuel an aircraft keeping the current kerosene turnaround times. The remaining flows correspond to intermediate values that could appear in the event that demand increases with respect to the average case.

Figure 4.14 shows the BO obtained for the different mass flows analyzed. It is appreciated a considerable increase in the total BO as the mass flow in the pipeline increases. Heat input BO remain the same in all cases, so the total increase is directly associated with an increase in friction between the fluid and the pipe wall. For the same pipe diameter, the higher the mass flow, the higher the fluid speed, and according to the *Darcy-Weisbach* formula, Equation (3.6), friction pressure losses are directly related to the square of the fluid speed. For this reason, an increase in both pump BO and friction BO is observed. The increase in the latter is especially important at 12 kg/s and above.

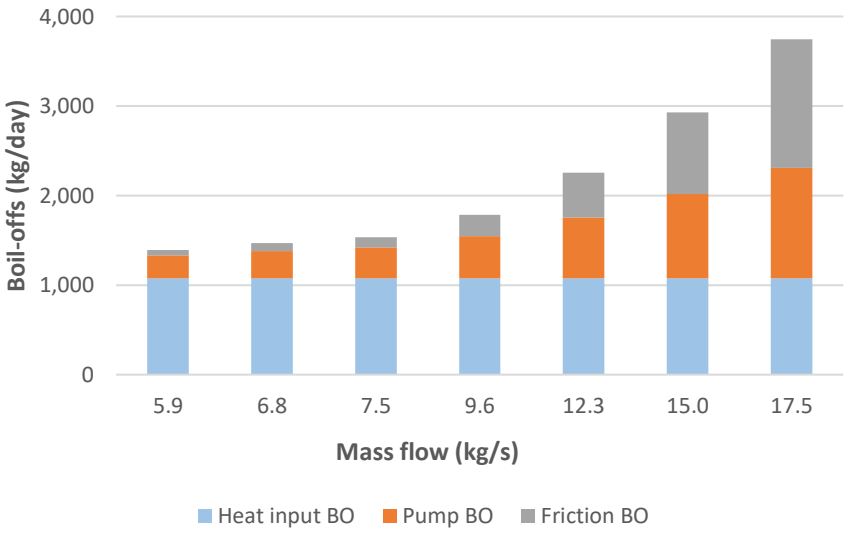

Figure 4.14: Comparison of daily boil-offs as a function of the mass flow through the distribution pipeline.

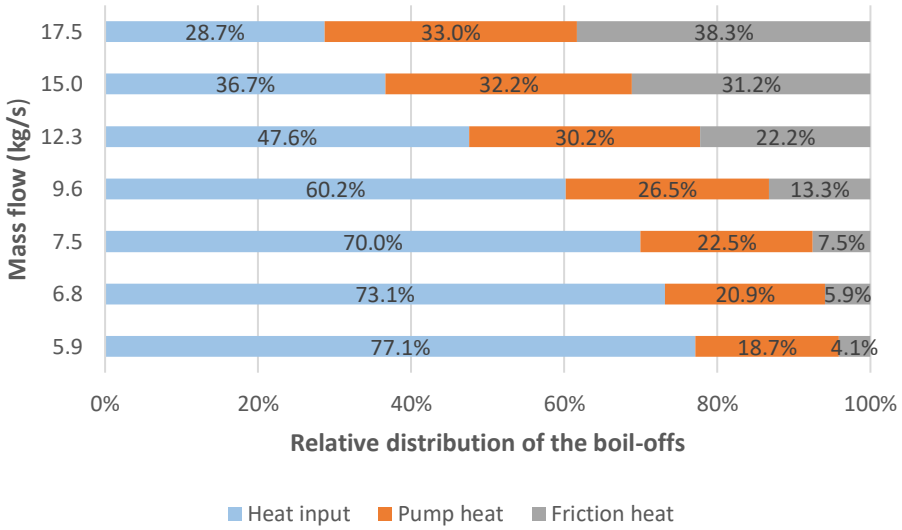

Figure 4.15: Distribution of boil-offs per heat source for different mass flows through the distribution pipeline.

Figure 4.15 shows that the friction BO becomes the majority group when the mass flow exceeds 15 kg/s, i.e., when the fluid speed is greater than 2.6 m/s. Following this trend, the higher the mass flow rate, the lower the contribution of heat input BO to the total BO comparatively.

Figure 4.16 shows the boil-off rates obtained for each mass flow. For the calculation of these values it is considered that the daily consumption does not vary with respect to the average case.

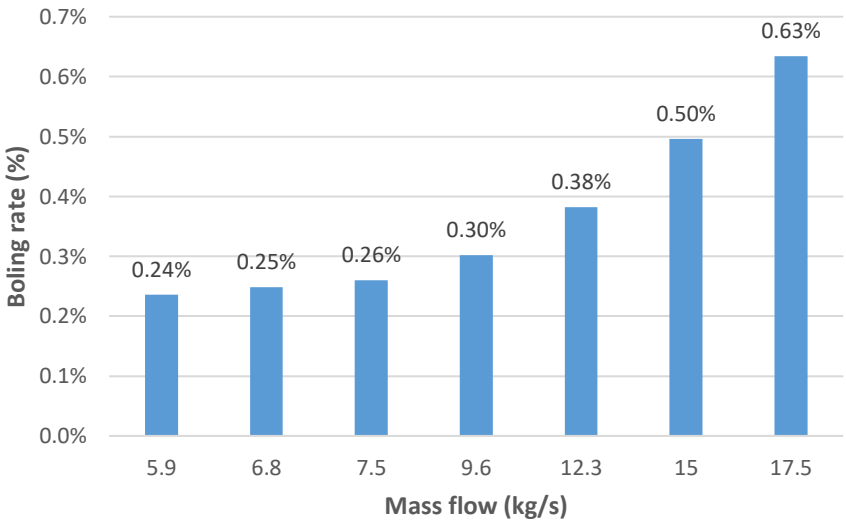

Figure 4.16: Resulting boil-off rates in the distribution system for each of the mass flows analyzed.

The resulting boil-offs from each heat category as a function of the mass flow and the variations with respect to the average case are shown in the following tables. Table 4.22 shows the results associated with the pumping group. Increased friction requires more pumping power and consequently considerably increases the heat transferred to the fluid. The percentage variations in both pump BO and pump characteristics are the same for each mass flow. As Table 4.22 shows, the increase in mass flow has a significant impact on the power of the pumping group required and consequently on the energy consumption of the installation. This results in higher construction and operating costs. For example, delivering a mass flow of 17.5 kg/s would require four times the power capacity in comparison with the average case.

Table 4.22: Comparison of pump BO and pump power depending on the mass flow and percentage variation with respect to the average case.

$\boldsymbol{Mass\ flow}$ $(\boldsymbol{kg/s})$	$\boldsymbol{Mass\ flow\ fraction}$	$\boldsymbol{Pump\ BO}$ $(\boldsymbol{kg/day})$	$\boldsymbol{Pump\ power}$ $(\boldsymbol{kW})$	$\boldsymbol{Variation\ from\ average\ case}$ (%)
5.94	0.87	261	4.99	-15.2
6.83	1	307	5.89	–
7.51	1.1	345	6.62	12.4
9.56	1.4	473	9.06	53.8
12.30	1.8	681	13.04	121.5
15.03	2.2	943	18.06	206.8
17.49	2.56	1,235	23.66	301.9

Table 4.23 shows the enormous impact of the mass flow on friction BO. The impact is so remarkable that working with a mass flow two and a half times higher than the average case, i.e, 17.5 kg/s, results in a friction BO volume more than sixteen time higher.

Table 4.23: Comparison of friction BO depending on the mass flow and percentage variation with respect to the average case.

$\boldsymbol{Mass\ flow}$ $(\boldsymbol{kg/s})$	$\boldsymbol{Mass\ flow\ fraction}$	$\boldsymbol{Friction\ BO}$ $(\boldsymbol{kg/day})$	$\boldsymbol{Friction\ BO\ variation\ from\ average\ case}$ (%)
5.94	0.87	57.53	-33.9
6.83	1	87.01	–
7.51	1.1	115.52	32.8
9.56	1.4	236.87	172.2
12.30	1.8	501.16	476

15.03	2.2	912.32	948.5
17.49	2.56	1,434.76	1,549

Finally, Table 4.24 shows the resulting total BO for each mass flow and the increments with respect to the base case. There is a noticeable increase in the BO when the mass flow through the pipeline increases. Therefore, the mass flow is so far the most influential factor on the boil-off rate of all the parameters analyzed.

Table 4.24: Comparison of total BO depending on the mass flow and percentage variation with respect to the average case.

$\boldsymbol{Mass\ flow}$ $(\boldsymbol{kg/s})$	$\boldsymbol{Mass\ flow\ fraction}$	$\boldsymbol{Total\ BO}$ $(\boldsymbol{kg/day})$	$\boldsymbol{Total\ BO\ variation\ from\ average\ case}$ (%)
5.94	0.87	1,392	-5.19
6.83	1	1,468	–
7.51	1.1	1,534	4.54
9.56	1.4	1,783	21.48
12.30	1.8	2,255	53.6%
15.03	2.2	2,929	99.52
17.49	2.56	3,743	155.02

4.3.5. Efficiency of the pumping group

The influence of the efficiency of the pumping group on the distribution system is studied. In this case, the only heat source affected by the parametric analysis is the pump heat. Therefore, heat input and friction BO will remain equal to the average case. The impact of the pump efficiency is analyzed for a series of values ranging from 75% to 105% with respect to the average case, which considers a 0.73 efficiency. Outside these values it is unlikely that the pump will operate, as full performance is impossible to achieve and working below a 0.5 efficiency would be unacceptable.

Figure 4.17 shows the BO obtained for the different efficiencies of the pumping group analyzed. As the pump performance improves, pump BO become smaller. It is also observed that, under the described conditions, the main BO are always associated with the heat input, even for the lowest pump performance. If the efficiency exceeds 0.85 the contribution of friction BO is greater than those of the pump. As shown in Figure 4.17, at the maximum efficiency studied, i.e., 0.95, BO associated with the heat pump are very small and represent only 3.7% of the total BO.

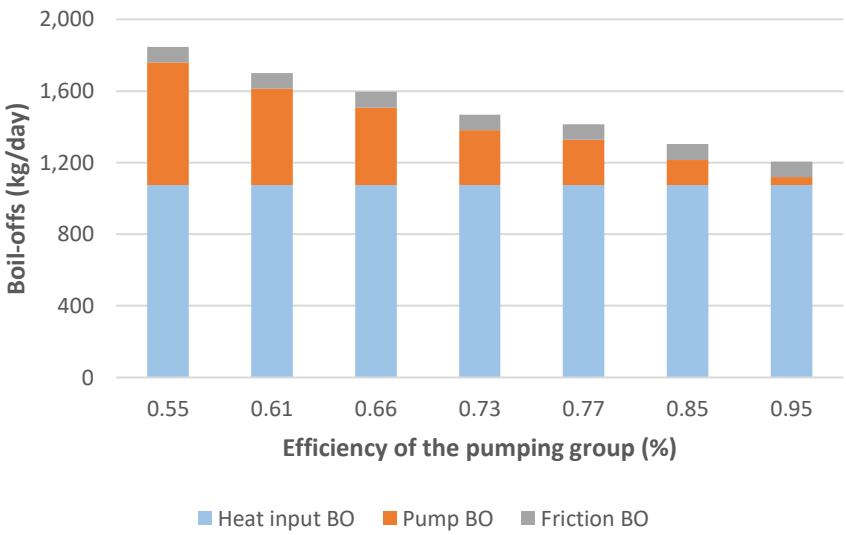

Figure 4.17: Comparison of daily boil-offs as a function of the pumping group efficiency.

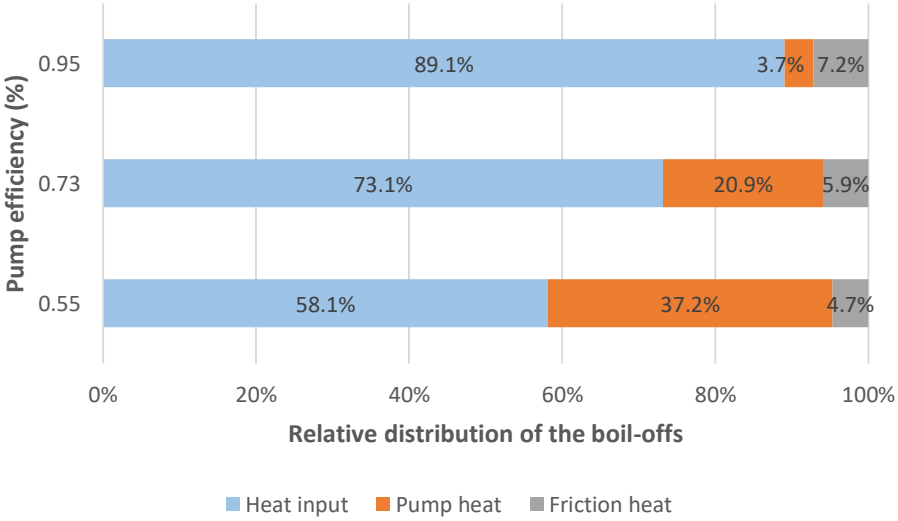

Figure 4.18: Distribution of boil-offs per heat source for different efficiencies of the pumping group.

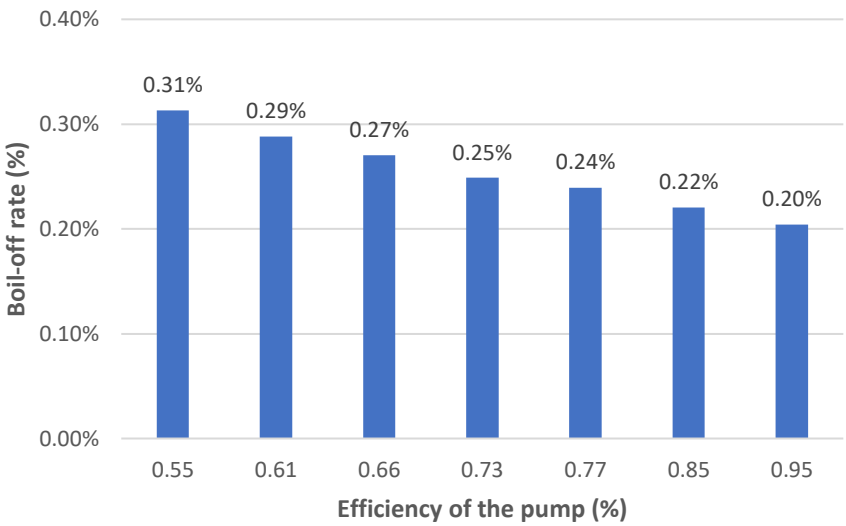

Figure 4.19: Resulting boil-off rates in the distribution system for each of the pump efficiencies analyzed.

The results of the BO as a function of the pump efficiency and the variations with respect to the average case are shown in the following tables. Table 4.25 shows the effects only on the pump BO, while Table 4.26 summarizes the impact of pump efficiency on the total boil-offs.

Table 4.25: Comparison of pump BO depending on the pump efficiency and percentage variation with respect to the average case.

$\boldsymbol{Pump\ efficiency}$ (%)	$\boldsymbol{Pump\ efficiency\ fraction}$	$\boldsymbol{Pump\ BO\ (kg/day)}$	$\boldsymbol{Pump\ BO\ variation\ from\ average\ case}$ (%)
0.55	0.75	687	123.5
0.61	0.83	540	75.9
0.66	0.9	434	41.2
0.73	1	307	–
0.77	1.05	253	-17.6
0.85	1.17	142	-53.8
0.95	1.3	45	-85.5

Table 4.26 reveals that the impact of the pump efficiency on the boil-offs is limited by the operating performance range of the pump. Efficiency may not fall below 0.55 or exceed 0.95, therefore, under any distribution scenario, the maximum decrease or increase in the total BO as a function of the pump efficiency will be between 25.8% and -17.9%,

respectively, with respect to the average case. For intermediate pump efficiency values, the impact on the total BO will be moderate.

Table 4.26: Comparison of total BO depending on the pump efficiency and percentage variation with respect to the average case.

$\boldsymbol{Pump\ efficiency}$ (%)	$\boldsymbol{Pump\ efficiency\ fraction}$	$\boldsymbol{Total\ BO}$ $(\boldsymbol{kg/day})$	$\boldsymbol{Total\ BO\ variation\ from\ average\ case}$ (%)
0.55	0.75	1,847	25.8
0.61	0.83	1,701	15.9
0.66	0.9	1,594	8.6
0.73	1	1,468	–
0.77	1.05	1,414	-3.7
0.85	1.17	1,302	-11.3
0.95	1.3	1,205	-17.9

Finally, the efficiency of the pump will affect the power required. The higher the efficiency, the lower the pump power. Consequently, energy consumption and operating costs would be lower. Table 4.27 shows the pumping unit power required for each of the efficiencies studied and the variation with respect to the average case.

Table 4.27: Comparison of the pump power required depending on the pump efficiency and percentage variation with respect to the average case.

$\boldsymbol{Pump\ efficiency}$ (%)	$\boldsymbol{Pump\ efficiency\ fraction}$	$\boldsymbol{Pump\ power}$ $(\boldsymbol{kW})$	$\boldsymbol{Pump\ power\ variation\ from\ average\ case}$ (%)
0.55	0.75	7.85	33.3
0.61	0.83	7.09	20.5
0.66	0.9	6.54	11.1
0.73	1	5.89	–
0.77	1.05	5.61	-4.8
0.85	1.17	5.03	-14.5
0.95	1.3	4.53	-23.1

4.3.6. Supply pressure at the transfer tank

The last parametric analysis studies the impact of the supply pressure at the transfer tank on the performance of the distribution system. According to various authors, the pressure in the transfer tank can range from 1.5 to 5 bar (Aziz, 2021; Silberhorn et al., 2019). A high pressure in the intermediate tank, within the above pressure range, favors the refueling of the aircraft by the pressure differential method. Therefore, the impact of the chosen supply pressure in the average case, i.e., 1.5 bar, is compared with a series of higher pressures, up to 5 bar. The performance and requirements of the distribution system under each supply pressure is analyzed and the resulting boil-offs are obtained.

Figure 4.20 shows that increasing the supply pressure in the transfer tank has a considerable impact on the BO. The higher the pressure demanded in the intermediate tank, the higher the BO. This increase is solely due to an increase in the heat added by the pumping group. The contributions from the other two heat sources, external heat and friction, remain the same as in the average case. As shown in Figure 4.20, pump BO become the majority group when the supply pressure exceeds 2.4 bar. As the required pressure increases friction BO can be considered negligible.

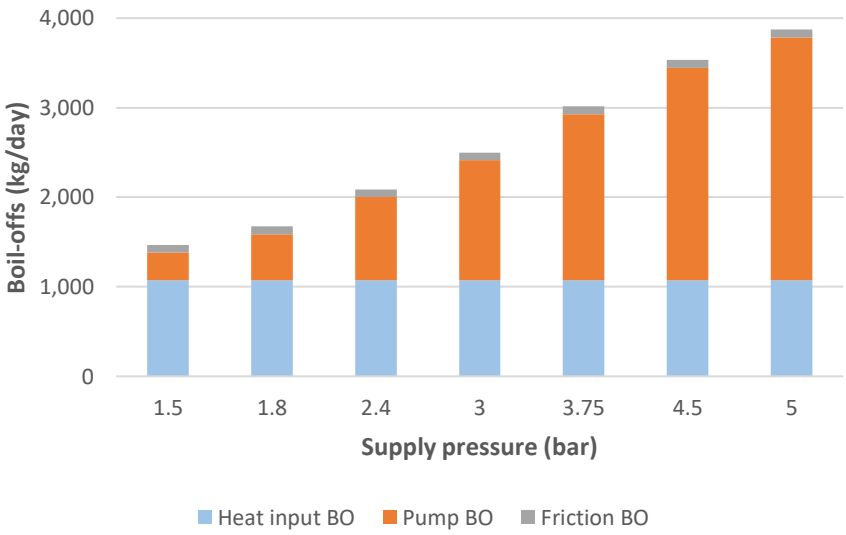

Figure 4.20: Comparison of daily boil-offs as a function of the supply pressure at the transfer tank.

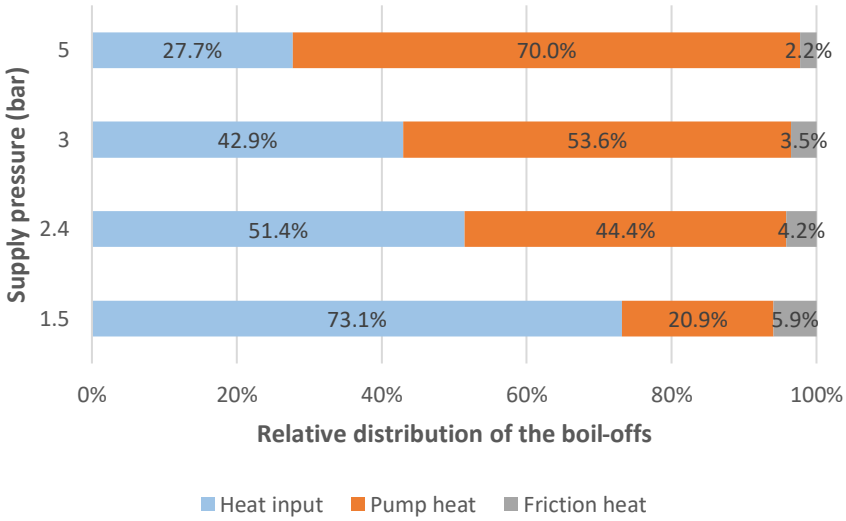

Figure 4.21: Distribution of boil-offs per heat source for different supply pressures at the transfer tank.

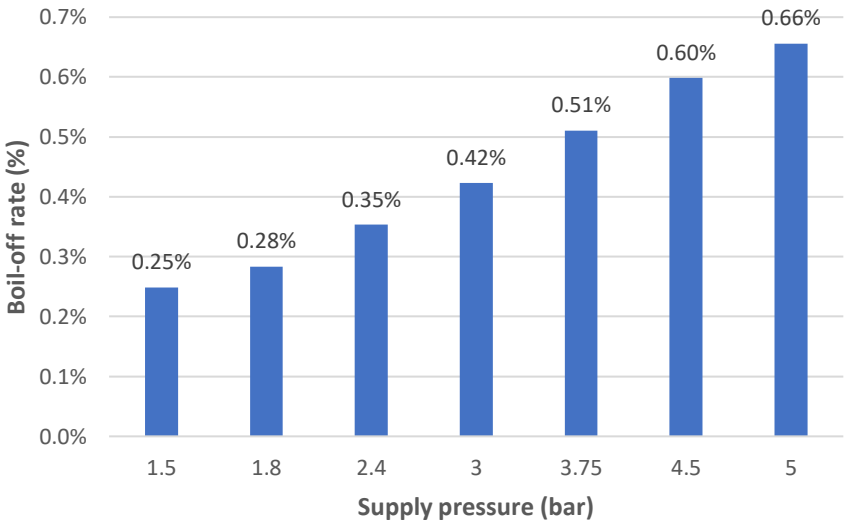

Figure 4.22: Resulting boil-off rates in the distribution system for each of the supply pressures analyzed.

The results of the BO as a function of the supply pressure at the transfer tank and the variations with respect to the average case are shown in the following tables. Table 4.28 shows the BO associated with the pump and the power capacity required to provide the pressure demanded at the transfer tank. These results are shown in the same table as the percentage variation with respect to average case is the same for both pump BO and pump power. In turn, Table 4.29 summarizes the impact of the supply pressure on the total boil-offs.

Table 4.28: Comparison of pump BO and pump power depending on the supply pressure and percentage variation with respect to the average case.

$\boldsymbol{Supply\ pressure}$ $(\boldsymbol{bar})$	$\boldsymbol{Pressure\ fraction}$	$\boldsymbol{Pump\ BO}$ $(\boldsymbol{kg/day})$	$\boldsymbol{Pump\ power}$ $(\boldsymbol{kW})$	$\boldsymbol{Variation\ from\ average\ case}$ (%)
1.5	1	307	5.9	–
1.8	1.2	514	9.8	67.1
2.4	1.6	926	17.8	201.4
3	2	1,339	25.7	335.7
3.75	2.5	1,855	35.5	503.6
4.5	3	2,371	45.4	671.5
5	3.33	2,711	52.0	782.3

Table 4.29: Comparison of total BO depending on the supply pressure and percentage variation with respect to the average case.

$\boldsymbol{Supply\ pressure}$ $(\boldsymbol{bar})$	$\boldsymbol{Pressure\ fraction}$	$\boldsymbol{Total\ BO}$ $(\boldsymbol{kg/day})$	$\boldsymbol{Total\ BO\ variation\ from\ average\ case}$ (%)
1.5	1	1,468	–
1.8	1.2	1,674	14.1
2.4	1.6	2,087	42.2
3	2	2,500	70.3
3.75	2.5	3,015	105.4
4.5	3	3,531	140.6
5	3.33	3,872	163.8

The two tables above show that increasing the supply pressure at the transfer tank leads to a large increase in total BO and requires a much more powerful pumping group than in the base case. This means higher energy consumption during operation of the installation. In addition, the higher the total volume of BO, the more difficulties associated with its handling, such as the need for larger recovery infrastructures, greater demand for space at the airport, security risks, etc.

5. Summary and Outlook

This work presents a simplified initial assessment approach to the distribution of liquid hydrogen via pipeline at airports. Special focus is given to the study of the boil-off phenomenon occurring over the distribution pipeline when transferring the LH_2 from the airport storage farm to the aircraft stand. First, a base case configuration of the distribution system is defined. It is decided to use one backbone pipeline branching to each aircraft stand. An intermediate tank is located at each stand to store the LH_2 before refueling. This design facilitates pressure control in the main pipeline and allows some decoupling between instantaneous demand and mass flow through the pipeline as the transfer tanks can buffer the demand. Thus, several aircraft can be refueled at the same time without affecting the mass flow and pressure within the main pipeline. Next, the main elements involved in the distribution system are identified. Along the described distribution scenario, three major causes of added heat are identified: the incoming heat from the outside, the heat supplied by the pump and the heat resulting from friction. Next, in order to allow insights into boil-off along the distribution chain, a simplified mathematical description is proposed. Based on that and on fundamental technology/material assumptions, boil-off occurring along the pipeline distribution system of a generic airport is obtained. In addition, several analyses of the effects of the parameters of the system on the boil-off are performed.

The results of each parametric analysis are compared to the base case and discrepancies are shown as percentage variations. The parameters analyzed are the insulation correction factor, the ambient temperature, the pipe length, the mass flow, the efficiency pump and the supply pressure at the stand tank. From the analysis it is concluded that there are certain parameters such as the pipe length, the mass flow delivered and the supply pressure at the stand tank that have special impact on the boil-off occurring along the pipeline distribution system. An increase in the pipe length linearly affects the heat input from the outside, which increases according to the increase in the pipe surface area. In turn, modifying the mass flow through the pipe has a great impact on the friction BO. Friction becomes particularly large when the fluid speed exceeds 2.6 m/s. Last, the supply pressure required significantly affects the heat contribution of the pumping group, which increases linearly as the pressure demanded grows. These findings give a first indication on the performance and sensitivities of a LH_2-based airport distribution system.

As mentioned, this simplified model comes with a number of limitations, which should be addressed by further research. The next step in academic research should be to develop a model that studies the behavior of liquid hydrogen in the pipeline more accurately. For example, it would be interesting to build a model that considers two-phase flow. Thus, the impact of boil-off gases on the temperature and pressure of the fluid along the pipeline could be analyzed. In this line, it would also be interesting to carry out an investigation on the possible alternatives to remove the boil-off gases from the distribution pipeline. Finally, as a continuation of this work, an economic study could be carried out to analyze the cost associated with the recovery and treatment of boil-off gases. In practice, much effort must be invested in the coming decades to develop the equipment and technologies that will enable hydrogen to be deployed in aviation.

Bibliography

Adler, Eytan & Martins, Joaquim. (2023). Hydrogen-Powered Aircraft: Fundamental Concepts , Key Technologies, and Environmental Impacts.

Adler, M., Peerlings, B., Boonekamp, T., Van Der Sman, E., Lim, N., Jongeling, A., & Pel, S. (2023). *The Price of Net Zero. Aviation Investments towards Destination 2050*.

URL: https://www.iata.org/en/pressroom/pr/2017-12-05-01/

Al Ghafri, S. Z., Munro, S., Cardella, U., Funke, T., Notardonato, W., Trusler, J. P. M., Leachman, J., Span, R., Kamiya, S., Pearce, G., Swanger, A., Rodriguez, E. D., Bajada, P., Jiao, F., Peng, K., Siahvashi, A., Johns, M. L., & May, E. F. (2022). Hydrogen liquefaction: a review of the fundamental physics, engineering practice and future opportunities. In *Energy and Environmental Science* (Vol. 15, Issue 7, pp. 2690–2731). Royal Society of Chemistry. Available from: https://doi.org/10.1039/d2ee00099g

Aziz, M. (2021). Liquid hydrogen: A review on liquefaction, storage, transportation, and safety. In *Energies* (Vol. 14, Issue 18). MDPI. Available from: https://doi.org/10.3390/en14185917

Boeing. (1976). *An Exploratory Study to Determine The Integrated Technological Air Transportation System Ground Requirements of Liquid-Hydrogen-Fueled Subsonic, Long-Haul Civil Air Transports National Aeronautics and Space Administration*.

Brewer, G. D. (1976). *LH2 Airport Requirements Study.* Prepared by Lockheed-California Co. NASA-CR-2700.

CaetanoBus. (2019). *H2 City Gold Bus*.

URL: https://caetanobus.pt/wp-content/uploads/2019/10/H2.City-Gold_ENG.pdf

DEMACO. (2018). *Product Sheet: Vacuum-Insulated-Piping*.

URL: www.demaco.nl

European Comission. (2019). *European Comission Green Deal*.

URL: https://commission.europa.eu/strategy-and-policy/priorities-2019-2024/european-green-deal/delivering-european-green-deal_en

European Union Aviation Safety Agency., & European Environment Agency. (2022). *European aviation environmental report 2022.*

Fesmire, J. E., & Swanger, A. (2021). *Overview of the New LH2 Sphere at NASA Kennedy Space Center*.

García, S. (2016). *Suministro por tubo de queroseno Coruña - Aeropuerto La Coruña*. Universidad Politécnica de Madrid.

Groznik, J. (2020). *Boil-off gas handling from liquefied hydrogen storage*.

H2 Tools. (2023). *Density of hydrogen*.

URL: https://h2tools.org/hyarc/hydrogen-data/hydrogen-density-different-temperatures-and-pressures

HFTO. (2023). Hydrogen Storage.

URL: https://www.energy.gov/eere/fuelcells/hydrogen-storage

Hoelzen, J., Flohr, M., Silberhorn, D., Mangold, J., Bensmann, A., & Hanke-Rauschenbach, R. (2022). 'H2-powered aviation at airports – Design and economics of LH2 refueling systems'. *Energy Conversion and Management: X*, *14*. Available from: https://doi.org/10.1016/j.ecmx.2022.100206

IATA. (2019). *Fact Sheet 7: Liquid hydrogen as a potential low-carbon fuel for aviation*.

URL: https://www.iata.org/contentassets/d13875e9ed784f75bac90f000760e998/fact_sheet7-hydrogen-fact-sheet_072020.pdf

IEA. (2019). *The Future of Hydrogen*.

URL: https://www.iea.org/reports/the-future-of-hydrogen

IEA. (2022). *Global Hydrogen Review 2022*.

URL: https://www.iea.org/reports/global-hydrogen-review-2022

IEA. (2023). *Greenhouse Gas Emissions from Energy Data Explorer*.

URL: https://www.iea.org/data-and-statistics/data-tools/greenhouse-gas-emissions-from-energy-data-explorer

Jovan, D. J., & Dolanc, G. (2020). Can green hydrogen production be economically viable under current market conditions. *Energies*, *13*(24). Available from: https://doi.org/10.3390/en13246599

Katebah, M., Al-Rawashdeh, M., & Linke, P. (2022). Analysis of hydrogen production costs in Steam-Methane Reforming considering integration with electrolysis and CO2 capture. *Cleaner Engineering and Technology*, *10*, 100552. Available from: https://doi.org/10.1016/j.clet.2022.100552

Kim, J. H., Park, D. K., Kim, T. J., & Seo, J. K. (2022). Thermal-Structural Characteristics of Multi-Layer Vacuum-Insulated Pipe for the Transfer of Cryogenic Liquid Hydrogen. *Metals*, *12*(4). Available from: https://doi.org/10.3390/met12040549

Kolodziejczyk, B. (2023). *How to understand the carbon footprint of clean hydrogen*.

URL: https://www.weforum.org/agenda/2023/03/understand-carbon-footprint-green-hydrogen/+

Lee, D. S., Fahey, D. W., Skowron, A., Allen, M. R., Burkhardt, U., Chen, Q., Doherty, S. J., Freeman, S., Forster, P. M., Fuglestvedt, J., Gettelman, A., De León, R. R., Lim, L. L., Lund, M. T., Millar, R. J., Owen, B., Penner, J. E., Pitari, G., Prather, M. J., … Wilcox, L. J. (2021). The contribution of global aviation to anthropogenic climate forcing for 2000 to 2018. *Atmospheric Environment*, *244*. Available from: https://doi.org/10.1016/j.atmosenv.2020.117834

Lopez, S. (2022). *Airport Infrastructure and Operations for Hydrogen Aircraft: A Model-Based Analysis*. Technical University of Munich.

Mangold, J., Silberhorn, D., Moebs, N., Dzikus, N., Hoelzen, J., Zill, T., & Strohmayer, A. (2022). Refueling of LH2 Aircraft—Assessment of Turnaround Procedures and Aircraft Design Implication. *Energies*, *15*(7). Available from: https://doi.org/10.3390/en15072475

McKinsey & Company for the Clean Sky 2 JU and Fuel Cells and Hydrogen 2 JU. (2020). *Hydrogen-powered aviation. A fact-based study of hydrogen technology, economics, and climate impact by 2050*. Available from: https://doi.org/10.2843/766989

Menon, E. Shashi. (2005). *Gas pipeline hydraulics*. Taylor & FRancis.

Mital, S. K., Gyekenyesi, J. Z., Arnold, S. M., Sullivan, R. M., Manderscheid, J. M., & Murthy, P. L. N. (2006). *Review of Current State of the Art and Key Design Issues With Potential Solutions for Liquid Hydrogen Cryogenic Storage Tank Structures for Aircraft Applications*.

URL: http://www.sti.nasa.gov

Mukhopadhaya, J., & Rutherford, D. (2022). *Performance Analysis of Evolutionary Hydrogen-powered Aircraft*.

URL: www.theicct.orgcommunications@theicct.org

Munich Airport. (2019a). *Environmental Statement 2019 Executive Summary. The Environment at Munich Airport*.

URL: https://www.munich-airport.com/_b/00000000000000007853899bb5dd4f69d/umwelterklaerung-environmental-statement-2019.pdf

Munich Airport. (2019b). *Traffic Report*.

URL: https://www.munich-airport.com/_b/00000000000000008065605bb5def6a5f/traffic-report-2019.pdf

Polizelli, M. A., Menegalli, F. C., Telis, V. R. N., & Telis-Romero, J. (2003). Friction Losses in Valves and Fittings for Power-Law Fluids. *Brazilian Journal of Chemical Engineering*, *20*(04), 455–463.

Postma-Kurlanc, A., Leadbetter, H., & Pickard, C. (2022). *HYDROGEN INFRASTRUCTURE AND OPERATIONS. Airports, Airlines and Airspace Aerospace Technology*.

Silberhorn, D., Atanasov, G., Walther, J.-N., & Zill, T. (2019). *Assessment of Hydrogen Fuel Tank Integration at Aircraft Level*.

StackExchange. (2021). *Dynamic viscosity of liquid hydrogen*.

URL: https://physics.stackexchange.com/questions/657431/viscosity-of-liquid-hydrogen-and-its-effect

Swanger, A. M. (2022). *World s Largest Liquid Hydrogen Tank Nearing Completion*. Available from: https://doi.org/10.1016/j.cryogenics.2017.10.008

Thomson, R., Weichenhain, U., & Kaufmann, M. (2020). *Hydrogen | A future fuel for aviation?*

URL: https://www.rolandberger.com/en/Insights/Publications/Hydrogen-A-future-fuel-for-aviation.html

United Nations. (2015). *Paris Agreement*.

URL: https://www.un.org/en/climatechange/paris-agreement

Verstraete, D. (2009). *The Potential of Liquid Hydrogen for long range aircraft propulsion*.

Weather Spark. (2023). Climate and Average Weather Year Round in Munich, Germany.

URL: https://weatherspark.com/y/70344/Average-Weather-in-Munich-Germany-Year-Round

Xu, W., Li, Q., & Huang, M. (2015). Design and analysis of liquid hydrogen storage tank for high-altitude long-endurance remotely-operated aircraft. *International Journal of Hydrogen Energy*, *40*(46), 16578–16586. Available from: https://doi.org/10.1016/j.ijhydene.2015.09.028

Declaration of Authorship

I hereby declare that the thesis submitted is my own unaided work. All direct or indirect sources used are acknowledged as references. I am aware that the thesis in digital form can be examined for the use of unauthorized aid and in order to determine whether the thesis as a whole or parts incorporated in it may be deemed as plagiarism. For the comparison of my work with existing sources I agree that it shall be entered in a database where it shall also remain after examination, to enable comparison with future theses submitted. Further rights of reproduction and usage, however, are not granted here. This paper was not previously presented to another examination board and has not been published.

Valencia, August 23, 2023

first and last name